N 63 13874

RM L57L03

NACA

RESEARCH MEMORANDUM

HEAT-TRANSFER MEASUREMENTS IN FREE FLIGHT AT MACH NUMBERS UP TO 14.6 ON A FLAT-FACED CONICAL NOSE WITH A TOTAL ANGLE OF 29°

By Charles B. Rumsey and Dorothy B. Lee

Langley Aeronautical Laboratory
Langley Field, Va.

Declassified February 8, 1963

NATIONAL ADVISORY COMMITTEE
FOR AERONAUTICS
WASHINGTON

January 24, 1958

NACA RM L57L03

NATIONAL ADVISORY COMMITTEE FOR AERONAUTICS

RESEARCH MEMORANDUM

HEAT-TRANSFER MEASUREMENTS IN FREE FLIGHT AT MACH NUMBERS UP TO 14.6 ON A FLAT-FACED CONICAL NOSE WITH A TOTAL ANGLE OF 29°

By Charles B. Rumsey and Dorothy B. Lee

SUMMARY

Skin-temperature measurements have been made at several locations on a flat-faced cone-cylinder nose which was flight tested on a five-stage rocket-propeller model to a Mach number of 14.64 and a free-stream Reynolds number of 2.0×10^6, based on flat-face diameter, at an altitude of 66,300 feet. The copper nose had a 29° total-angle conical section which was 1.6 flat-face diameters long. The aerodynamic-heating rates determined from the temperature measurements reached 1,440 Btu/(sec)(sq ft) on the flat face.

The heating rates near the center of the flat face agreed well at Mach numbers up to 13.6 with those obtained by a theory for laminar stagnation-point heating in equilibrium dissociated air (AVCO Res. Rep. 1). At Mach numbers above 13.6, the heating rates at locations near the center of the flat face became progressively lower than stagnation-point theory and were 29 percent lower at Mach number 14.6 at the end of the test. The reason for this behavior of the heating on the central part of the flat face was not determined.

Excluding the relatively low heating rates that occurred on the central part of the nose at the highest Mach numbers, the distribution of experimental heating along the innermost 0.79 of the flat-face radius, expressed as a percentage of stagnation-point heating, was in fair agreement with the distribution predicted by laminar theory. At a location of 0.71 radii from the stagnation point, the experimental heating was very near 130 percent of the theoretical stagnation-point rate at Mach numbers from 11 to 14.5.

The experimental heating rates on the conical section of the nose were in good agreement with laminar-cone theory using the assumption of theoretical sharp-cone static pressure on the conical section.

INTRODUCTION

Aerodynamic heating on the noses of bodies flying at hypersonic speeds is currently being investigated by the Langley Pilotless Aircraft Research Division. Multistage rocket-propelled models are used to obtain hypersonic Mach numbers over a considerable range of altitudes and test trajectories.

Two investigations of the heating on a flat-faced cylinder have been made at Mach numbers up to 13.9 (ref. 1) and at Mach numbers up to 10.9 at a much increased maximum Reynolds number (ref. 2). Similar five-stage models were used in both tests. The heat transfer on a 29° total-angle conical nose blunted with a hemispherical tip has also been measured at Mach numbers up to 15.5 and is reported in reference 3.

In the present test, skin-temperature measurements were made at several locations on a flat-faced cone-cylinder nose with a low fineness ratio. The conical section had a total angle of 29° and was 1.6 flat-face diameters long. Noses of this general type are of interest in application where the high drag of a blunted cylindrical nose is undesirable. This test also utilized a five-stage model similar to those of references 1 to 3. Heat-transfer data were obtained and are herein presented for Mach numbers from 3.3 to 14.64 with corresponding free-stream Reynolds numbers from 0.14×10^6 to 1.92×10^6, based on flat-face diameter. The altitude of maximum Mach number was 66,300 feet. The flight test was conducted at the Langley Pilotless Aircraft Research Station at Wallops Island, Va., on May 16, 1957. The fourth-stage rocket motor (JATO, 1.52-KS-33550, XM-19 (Recruit)) used in the present investigation was made available by the U. S. Air Force.

SYMBOLS

a	speed of sound, ft/sec
A_{n+1}	contact area between elements n and n + 1, sq ft
A_{n-1}	contact area between elements n and n - 1, sq ft
C_p	specific heat of air, Btu/(lb)(°F)
C_N	normal-force coefficient, $\frac{\text{Normal force}}{\frac{1}{2}\rho_\infty U_\infty S}$

d	flat-face diameter, ft
h	enthalpy, Btu/lb
h_t	total enthalpy, Btu/lb
k	conductivity of air, (Btu)(ft)/(sec)($^\circ$F)(sq ft)
k_s	conductivity of wall material, (Btu)(ft)/(sec)($^\circ$F)(sq ft)
M	Mach number
N_{Nu}	Nusselt number
N_{Pr}	Prandtl number
p	pressure, lb/(sq ft)
q	heating rate, Btu/(sec)(sq ft)
r	radius of flat face, ft
R_d	free-stream Reynolds number based on flat-face diameter, $\frac{\rho_\infty U_\infty d}{\mu_\infty}$
R_w	local Reynolds number at wall conditions, $\frac{\rho_w U_l x}{\mu_w}$
R_θ	local Reynolds number based on boundary-layer momentum thickness, $\frac{\rho_l U_l \theta}{\mu_l}$
S	cross-sectional area of cylindrical part of body, 0.1963 sq ft
S_n	area of element n exposed to air flow, sq ft
T	temperature, $^\circ$R unless otherwise noted
t	time, sec
U	velocity, ft/sec

x	distance along nose surface from center, ft
Δx_{n+1}	distance between thermocouple locations in element n and n + 1, ft
Δx_{n-1}	distance between thermocouple locations in element n and n - 1, ft
α	angle of attack, deg
ρ	density of air, slugs/cu ft
τ	skin thickness, ft
μ	absolute viscosity of air, slugs/ft-sec

Subscripts:

l	local, outside boundary layer
o	at stagnation point
w	at temperature of wall
∞	free stream

MODEL AND TESTS

Model Configuration

The model was a body of revolution $63\frac{7}{8}$ inches long, with a flat-faced, 29° total-angle, cone-cylinder nose, a stepped cylindrical mid-section, and a 20° total-angle conical frustum at the rear. The general configuration is shown in figure 1(a), and pertinent dimensions are given in figure 1(b). Except for the nose shape, the model was similar to those used in the investigations of references 1, 2, and 3.

The nose was machined from a solid piece of electrolytic copper, and the dimensions are given in figure 2. The wall thickness was nominally 1/4 inch for the flat face and somewhat thinner along the conical and cylindrical sections. The measured wall thicknesses are given in the table in figure 2.

The copper nose was in contact with other parts of the model only at the base where a threaded steel ring was attached to it. Heat

conduction through this joint was minimized by a Micarta sleeve between the copper skin and the steel ring.

No particular effort was made to attain a high quality surface finish on the copper nose. After buffing with jewelers' rouge, the surface roughness was estimated by the use of an interference microscope at 15 to 20 microinches with several fine scratches which were doubtless much deeper than 20 microinches.

Three constant voltages were also commutated on each of the thermocouple telemeter channels. The constant voltages were chosen to be equivalent to the lowest, middle, and highest temperatures anticipated (from 80° to 1,900° F) and provided an inflight calibration of the thermocouple telemetering system.

Longitudinal acceleration was measured continuously by two accelerometers, each calibrated in gravitational units to cover the anticipated range of accelerations from a deceleration of 40g units to an acceleration of 150g units. Duplicate measurements of acceleration were made to provide an alternate in case of failure of one, since velocity during the high-speed portion of the flight was obtained solely by integration of longitudinal acceleration. Normal and transverse accelerations were measured continuously by the remaining two accelerometers which were each calibrated for accelerations of ±25g units.

Other instrumentation consisted of a CW Doppler radar velocimeter to provide velocity data during the earlier part of the test and an NACA modified SCR-584 tracking radar to provide the time history of the location of the model in space. Rawinsonde measurements provided atmospheric conditions and wind data at altitudes up to 90,000 feet. These measurements were made at the altitude of the high-speed portion of the flight within an hour of the flight test.

A radiation shield was located 3/16 inch inside the nose skin to protect instruments and equipment from the high skin temperatures expected; for the same reason, the cylindrical section behind the nose where most of the telemetering equipment was located was of double-walled construction. A short 20° total-angle conical frustum joined the forward cylindrical section with the larger rear section which contained the fifth-stage rocket motor. The 20° total-angle conical frustum at the rear of the model provided aerodynamic stability and also acted as an extension to the rocket nozzle.

Instrumentation

Measurements from 16 thermocouples and 4 accelerometers were telemetered during the test. The thermocouples, which were made of No. 30 chromel-alumel wire, were peened into shallow holes drilled into the inside surface of the copper nose skin at the locations shown in figure 2. Thirteen of the thermocouples were located inline from the stagnation point along an element of the nose. To check the symmetry of the heating, there were three thermocouples on the flat face each equidistant from the stagnation point and two on the conical frustum at diametrically opposite locations.

Two telemeter channels were used to transmit the measurements of the 16 thermocouples. The commutation arrangement was such that each of eight thermocouples were sampled approximately 10 times per second and the other eight were sampled half as often. This system allowed the use of more thermocouples since only 12 could have been used sampling all at the faster rate. The thermocouples sampled at the slower rate are indicated in figure 2.

Test Technique

The propulsion system consisted of five stages of solid-fuel rocket motors. The model, which contained the fifth-stage rocket motor, and the four booster stages are shown on the launcher in figure 3. The characteristics of the rocket motors are tabulated in reference 2, and the weights of each of the five stages of that test are also tabulated therein and are similar to those of the present investigation.

The model-booster combination was launched at an elevation angle of 74° and followed the trajectory shown in figure 4. The second stage was fired soon after burnout and drag separation of the first stage. After burnout and drag separation of the second stage, the remaining three stages coasted upwards to a peak altitude of 93,120 feet. When the flight path reached a reentry angle of about -25°, the third, fourth, and fifth stages were fired in rapid succession. The maximum Mach number of 14.64 occurred at an altitude of 66,300 feet. Very shortly thereafter, at burnout of the fifth-stage motor, the telemeter signal ended.

The time histories of velocity and altitude are shown in figure 5. The trajectory and altitude data of figures 4 and 5 were supplied by NACA modified SCR-584 tracking radar at times up to 102 seconds just after firing of the fourth stage. These data were extended to the time of telemeter failure, 105.5 seconds, by computations using the telemetered longitudinal accelerations. The velocity data were obtained

from CW Doppler radar at times up to 27.5 seconds, from differentiation of 584 radar data from 20.5 to 97 seconds, and from integration of the longitudinal accelerometers from 97 to 105.5 seconds.

Because of poor accuracy associated with the low rates of aerodynamic heating that occurred during the earlier portions of the test, only the heat-transfer data obtained during the high-speed reentry portion of the trajectory after 99 seconds are considered herein. The test conditions for this part of the flight are given in figures 6 and 7 which show the variations of velocity, altitude, Mach number, free-stream Reynolds number based on flat-face diameter, and the ambient values of velocity of sound, density, temperature, and pressure as functions of time.

Accuracy

The possible error in Mach number at the time of third-stage ignition is estimated to be about ±0.1. After third-stage ignition, velocity was obtained by integration of acceleration, and errors could be accumulative. Based on a comparison of the data from the two individual accelerometers, the accuracy of the velocity change from third-stage ignition to the end of the test is estimated to be within about 500 ft/sec. This results in a possible error in Mach number of about ±0.6 at the end of the test.

The measured temperatures are believed to be accurate within ±1 percent of the full-scale range of the temperature instrumentation, which amounts to an accuracy of ±19° F.

DATA REDUCTION

The basic heating data of the test are the thermocouple measurements of skin temperature. Figure 8 shows the skin-temperature measurements for stations 3 and 13, the hottest and coolest, respectively, of the measurement stations. The telemetered data are indicated by the symbols. The lines were faired through the data by hand and French curve and are the basis for the computation of the local heat rates.

At about 102.5 seconds, approximately midway through fourth-stage burning, the thermocouple commutating switch stopped due to the high longitudinal acceleration which reached a value of 145g units. When the acceleration decreased near burnout of the stage, the switch again began to rotate and operated normally thereafter. While the switch was stopped, from about 102.5 to 103.65 seconds, only the measurements from thermocouple 10_a, which transmitted continuously, were obtained. This

explains the lack of data in figure 8 during this time period. Although the curve faired smoothly in each case through this period of no data, the accuracy of the heat-transfer data between 102.4 and 103.75 seconds is questionable except for station 10_a.

Values from the faired curves of inside wall temperature are given for each measurement station at 0.2-second intervals in table I so that others may compare their methods of temperature prediction with the data of this test.

The aerodynamic-heating rates for each station were computed from the faired curves of inside wall temperature by first making a one-dimensional thick-wall heat-flow analysis by the method of reference 4 and then correcting the one-dimensional results for the lateral heat flow caused by the temperature gradients along the skin. It was not necessary to include the heat-flow rates due to external and internal radiation in the computations since these were completely negligible during this test.

In order to determine the one-dimensional heating rates, outside surface temperatures were first computed. By the method of reference 4, these heating rates are determined at successive regularly spaced time intervals from the inside surface temperatures at the preceding times and the thickness and material properties of the skin. Figure 9 shows the results of these computations for thermocouples 3_a and 13. The solid curves are the faired time histories of inside skin temperature shown in figure 8, and the symbols show the computed values of outside wall temperature, which were faired smoothly as indicated by the broken curve. At 105.45 seconds, the outside surface temperature at station 3 was 197° higher than the inside temperature, whereas at station 13 the difference was only 12°.

The one-dimensional heating rates were then computed from the faired time histories of outside wall temperature by means of the computational procedure of reference 4. This analysis considers only the heat flow normal to the skin.

Correction of the one-dimensional heat rates to account for the lateral heat-flow rates was necessary because of the large lateral temperature gradients in the skin which are apparent from the plots of temperature as a function of position shown in figure 10. The plotted values are the average temperatures through the wall, which was assumed to be the inside temperature plus one-third the difference between outside and inside temperature. This assumption is correct for a linear increase in heating rate with time. In order to aid in differentiating between the several sets of data, straight lines are used to connect values for a particular time. The method used to compute the lateral

heat-flow rates from these lateral temperature distributions was similar to that used in reference 1. The nose was divided into annular rings, one for each thermocouple location, and the temperature of each ring was assumed to be the average temperature at the thermocouple location. The lateral heat-flow rates were then computed for the annular ring n by the equation

$$q_{n,\text{lateral}} = \frac{k_s A_{n-1}(T_n - T_{n-1})}{S_n \Delta x_{n-1}} + \frac{k_s A_{n+1}(T_n - T_{n+1})}{S_n \Delta x_{n+1}} \qquad (1)$$

where $q_{n,\text{lateral}}$ is given in Btu/(sec)(sq ft). The contact areas A_{n-1} and A_{n+1}, the lengths Δx_{n-1} and Δx_{n+1} to the adjacent thermocouples, and the area of the ring exposed to the air flow S_n were determined from the dimensions of the nose and annular rings. The sizes of the rings were chosen so that the distance between thermocouples was equally divided. At the corner of the nose, the dividing surface common to the outermost ring of the flat face and the first ring of the conical section was taken to intersect the inside and outside corners of the skin; otherwise, all the dividing surfaces were normal to the skin.

This method of computing the lateral heat-flow rates is an approximation but is believed to be better than a computation using the differential form of the equation

$$q_{n,\text{lateral}} = -k_T\left(\frac{d^2T}{dx^2} + \frac{1}{x}\frac{dT}{dx}\right) \qquad (2)$$

because evaluation of $\frac{dT}{dx}$ and $\frac{d^2T}{dx^2}$ is critically dependent on the particular fairing that is put through the rather widely spaced measurements.

Equation (1) is an approximation also in the sense that lateral gradients of average wall temperature are used to determine the heat flow, although the flow is caused by the lateral gradients of the actual temperatures through the skin. It is believed that the simplifying assumption of average temperatures gives reasonably accurate lateral heat-transfer rates for all the measurement stations, excepting the ones adjacent to the corner. At these two stations, thermocouples 4 and 5, the accuracy of the computed lateral rates is very questionable; however, a more exact method for considering the heat flows near the corner from the limited data has not yet been determined.

The experimental aerodynamic heat-transfer rates were determined by adding, algebraically, the lateral heat-flow corrections for each station to the corresponding one-dimensional heat-flow rates.

RESULTS AND DISCUSSION

Experimental Heating Rates

The experimental heating rates for the 13 inline stations along the nose are shown in figure 11. The data points are given for both the one-dimensional heating rates and the aerodynamic-heating rates in order to show the amount of scatter in the results and to show the magnitudes of the computed lateral heat flows.

The aerodynamic-heating rates at both stations 1 and 2, in the central part of the flat face, decreased unexpectedly near 105 seconds, when the Mach number and ambient density were both increasing. This will be discussed later in the comparison of experimental and theoretical stagnation-point heating.

The maximum aerodynamic-heating rate was 1,440 Btu/(sec)(sq ft). It occurred at station 3_a, although station 4 which is closer to the corner would be expected to have the highest rate. It may be noted that the apparent rates are quite similar for the two stations, and the doubtful accuracy of the lateral heat-flow term for station 4, may be at least partly responsible for the lower aerodynamic heating shown for station 4.

Negative aerodynamic heating is shown for station 6 before 100.4 seconds and for station 7 near 102 seconds. However, the lateral flow-rate corrections, which give these negative values, result from temperature differences between the adjacent stations of less than 10° F. This is within the accuracy of the temperature measurements, and it is not believed that negative aerodynamic heating actually occurred.

The heating rates on the conical section, stations 5 to 11, are much less than those on the flat face as would be expected. Similarly, those on the cylindrical section, stations 12 and 13, are lower yet. The rates are compared with theory in subsequent figures.

Stagnation-Point Heating

The experimental aerodynamic heating for station 1, which is 1/8 inch from the center of the flat face, is compared in figure 12

with the theory of Fay and Riddell for laminar stagnation-point heat transfer in dissociated air (ref. 5). Their result for laminar stagnation-point heat-transfer rate is

$$q_o = \frac{N_{Nu}}{\sqrt{R_w}} \frac{\sqrt{\rho_w \mu_w \left(\frac{dU}{dx}\right)_o}}{N_{Pr}} \left(h_t - h_w\right) \tag{3}$$

where

$$\frac{N_{Nu}}{\sqrt{R_w}} = 0.67 \left(\frac{\rho_o \mu_o}{\rho_w \mu_w}\right)^{0.4} \tag{4}$$

for the assumptions of equilibrium dissociation, Lewis number of one, and Prandtl number of 0.71.

Density and temperature were evaluated for the test conditions by use of the perfect gas (constant C_p) relations of reference 6. Sutherland's viscosity formula was used which Fay and Riddell (ref. 5) state is accurate within 10 percent for equilibrium air at temperatures below 16,200° R. As noted in reference 1, $\rho\mu$ values calculated with the use of perfect gas relations result in heating rates only 2 to 3 percent lower than those obtained by the use of the values of $\rho\mu$ that Fay and Riddell give for equilibrium dissociation.

The term $\left(\frac{dU}{dx}\right)_o^{1/2}$ was computed using the relation $\frac{r}{a_o}\left(\frac{dU}{dx}\right)_o = 0.3$, invariant with Mach number, which was obtained in reference 1 from a flat-face pressure distribution for $M = 1.5$. As discussed therein, an invariant value of $\frac{r}{a_o}\left(\frac{dU}{dx}\right)_o$ is equivalent to a distribution of $\frac{p}{p_o}$ near the stagnation point which is also constant with Mach number, and the value 0.3 yields a ratio of flat face to hemisphere stagnation-point heating of 0.5 for Mach numbers above 4.

Figure 12 shows that at Mach numbers up to 13.6 the theoretical laminar stagnation-point heating rates were in fair agreement with, though generally slightly below, the experimental heating rates for station 1, which is 1/8 inch from the center of the nose. The irregularity in the theoretical curve near 103.7 seconds resulted from an irregularity in the Mach number curve at this time, and does not appear in the experimental data because a perfectly smooth skin-temperature curve was faired through the time period 102.5 to 103.65 seconds, when no temperature measurements were obtained.

As was noted previously, the experimental aerodynamic-heating rates at station 1 unexpectedly decreased at about 104.85 seconds when the Mach number and ambient density were both increasing. In figure 12, the rates for station 1 are seen to fall 29 percent below the theoretical stagnation-point rate at 105.3 seconds when the Mach number was 14.6. The heating rates at station 2 also decreased shortly after 105 seconds as was shown in figure 11(a), and the magnitudes of the heating rates at these two stations near the center of the nose were very similar during this later part of the test.

Because the temperature and pressure on the flat face were fairly high (about 900° F and 175 lb/sq in., respectively) by 105 seconds and because the flat face was not internally supported, the possibility of plastic deformation of the nose was considered. An analysis of the deflection at the center of the nose was made by the Langley Dynamic Model Engineering Section. Although only approximate methods for analyzing this nose configuration could be found, the results indicated that the deflection should be well within the elastic rather than the plastic range at 105 seconds. This would mean a deflection of only a few hundredths of an inch at the stagnation point. On the basis of available information, such a deflection would not account for the difference between stagnation-point theory and experiment, and the difference is as yet unexplained.

Heating on the Flat Face

The distribution of experimental aerodynamic heating across the flat face is shown in figure 13. Data obtained at Mach numbers of 11 to 14.5 are shown. For lower Mach numbers, either the skin-temperature measurements were lacking or the heating rates were too low to have a reasonable percent accuracy.

The experimental data are divided by the theoretical stagnation-point values of Fay and Riddell (ref. 5). (See fig. 12.) Also plotted are curves for flat-face heating obtained from the theories of Stine and Wanlass (ref. 7) and Lees (ref. 8) divided in each case by their own stagnation-point values. These curves were presented in reference 1. They are based on the pressure distribution for a Mach number of 1.5 shown in reference 1 and on flow conditions for a Mach number of 1.5. Using flow conditions for a Mach number of 10 and the pressure distribution for a Mach number of 1.5 makes only a small change in the curve for values of x/r less than 0.9. It should be noted that these curves do not indicate the magnitude of heating predicted by the theories. Their purpose is to show theoretical distributions of heating across the face in terms of their stagnation-point magnitude.

Figure 13 shows that the experimental data at station 1 are within about 10 percent of those obtained by the stagnation-point theory of Fay and Riddell (ref. 5), except at the highest Mach numbers, 14 and 14.5. At these Mach numbers, the heating rates are as much as 29 percent lower than stagnation-point theory over the innermost 0.4 of the flat-face radius; however, the heating at stations 3 and 4, as a function of stagnation-point rate, shows no consistent change at the highest Mach numbers.

In general, the experimental heating rates shown in figure 13 increase with distance from the stagnation point. At station 3, 0.71 radii from the stagnation point, they are about 130 percent of the theoretical stagnation-point values and are in better agreement with the distribution curve of the theory of Stine and Wanlass (ref. 7) than that of the theory of Lees (ref. 8). (The data for station 3 should be given more weight than those for station 4 because of the questionable accuracy of the computed lateral heat flows for station 4.) However, measurements were not made close enough to the corner of the flat face to appraise the theoretical distributions where the two are significantly different.

The experimental distribution shows that boundary-layer transition did not take place along the innermost 0.8 of the flat-face radius. Transition would not be expected on the flat face since the maximum value of R_θ at the corner of the face was only 105 at a Mach number of 14.6 at 105.5 seconds.

Heating on the Sides of the Nose

Figure 14 shows the distributions of experimental heating along the surface of the nose for Mach numbers of 11 and 14.5 divided by theoretical stagnation-point heating. On the conical section, the experimental heating was 0.2 to 0.4 and on the cylindrical section about 0.1 of the theoretical stagnation-point values.

The experimental heating rates for the measurement stations on the conical and cylindrical sections of the nose are plotted against x/r in figure 15 for Mach numbers from 11 to 14.5. Distributions of theoretical heating rates, computed from the laminar and turbulent flat-plate and laminar-cone theories of reference 9 are also shown. The local Reynolds number was based on length along the surface from the stagnation point. Local conditions were determined using the total pressure behind the normal shock, and the static pressures on the conical and cylindrical sections were assumed to be theoretical sharp-cone pressure and free-stream static pressure, respectively. With this assumption of theoretical cone pressure on the conical section, the maximum local Reynolds number at the end of the conical section was 0.39×10^6 at $M = 14.5$.

On the conical section, the data are very much below the theoretical turbulent flat-plate magnitude. At each Mach number, the agreement with theoretical laminar-cone rates (laminar flat-plate values times $\sqrt{3}$) is surprisingly good, considering the actual nose shape.

On the cylindrical section, both the laminar and turbulent theoretical heating rates are so low that the scatter of the data covers both.

Angle of Attack and Symmetry of Heating

Since the symmetry of the heating on a body is sensitive to angle of attack, a normal and a transverse accelerometer were included in the instrumentation to measure the forces on the model perpendicular to the longitudinal axis. Data from these instruments showed that, just after separation of the model from the fourth-stage booster at 103.83 seconds, a resultant acceleration of 1 g existed which increased to 7.5g at the end of the test. The normal-force coefficients C_N, computed from the time histories of acceleration, model weight, and dynamic pressure, varied between 0.07 and 0.10, based on cross-sectional area of the model body (6-inch diameter). Using an estimated value of $dC_N/d\alpha$ of 0.0709 per degree, the calculated angles of attack vary between 1° and $1\frac{1}{2}^\circ$, at times after 103.83 seconds.

The circumferential orientation of the plane of the angle of attack placed the downwind element of the nose always within 40°, and generally within 20°, of the axial line of 13 thermocouples.

In order to determine the symmetry of the heating around the nose, three thermocouples were located on the flat face equidistant from the stagnation point, and two were located at diametrically opposite locations on the conical section. Two of these, 3_a on the flat face and 10_a on the cylindrical section, were part of the axial line of 13 thermocouples which provided the data previously discussed.

Figure 16 shows the location of the duplicate thermocouples and the curves faired through the measurements of inside surface temperature for each location. The data for station 10_a were continuous, whereas the others did not record during the time period indicated.

The temperatures at the three stations on the flat face differ by a maximum of 55° F, with station 3_a being the coolest. On the conical section, station 10_a was the hottest by a maximum of 30° F, but station 10_b heated more rapidly after about 104 seconds.

Figure 17 compares the heating rates at the duplicate stations. Lateral heat-flow computations could not be made for the stations not in the axial line of thermocouples since the temperature gradients along the skin were unknown; therefore, one-dimensional heating rates are compared, with the expectation that a comparison of aerodynamic-heating rates would show similar differences.

On the flat face, station 3_a had the lowest one-dimensional heating rate and, except for the period from 104 to 104.5 seconds, station 3_b, diametrically opposite, had the highest. The greatest difference after the time of no temperature data was about 20 percent. Station 3_a with the lower heating rate was on the downwind side of the nose. If the assumption is made that the lateral heat-flow rates at station 3_b were the same as those at station 3_a, the ratio of aerodynamic heating to theoretical stagnation-point heating for station 3_b would vary from 1.34 to 1.50 on the flat-face distribution plot of figure 12. This would be higher than the theoretical distribution curve of Stine and Wanlass (ref. 7) at that station by as much as 25 percent of the stagnation-point rate. It appears that, at small angles of attack, the heating rates on a flat face, as a function of stagnation-point rate, can increase more rapidly with distance from the stagnation point than is predicted by the theoretical distribution of Stine and Wanlass (ref. 7).

Figure 17 also shows that the heating rates on the conical section were up to 100 percent higher at station 10_b on the upwind side of the nose than at station 10_a. Although they may be indicative of transitional flow, these higher heating rates are not as high as the theoretical flat-plate turbulent magnitude, as is shown in figure 15.

CONCLUDING REMARKS

Skin-temperature measurements have been made at several locations on a flat-faced cone-cylinder nose which was flight tested on a five-stage rocket-propelled model to a Mach number of 14.64 and a free-stream Reynolds number of 2.0×10^6, based on flat-face diameter, at an altitude of 66,300 feet. The copper nose had a 29° total-angle conical section which was 1.6 flat-face diameters long. The aerodynamic-heating rates determined from the temperature measurements reached a maximum of 1,440 Btu/(sec)(sq ft) on the flat face.

The heating rates at a location close to the center of the flat face agreed well at Mach numbers up to 13.6 with those obtained by a theory for laminar stagnation-point heating in equilibrium dissociated air (AVCO Res. Rep. 1). At Mach numbers above 13.6, the heating rates

at locations near the center of the flat face became progressively lower than stagnation-point theory and were 29 percent lower at Mach number 14.6 at the end of the test. The reason for this behavior of the heating on the central part of the flat face was not determined. The heating at locations farther from the stagnation point did not show this change in trend at the highest Mach numbers.

Excluding the relatively low heating rates that occurred near the stagnation point at Mach numbers above 13.6, the distribution of experimental heating along the innermost 0.71 of the flat-face radius, expressed as a percentage of stagnation-point heating, was in fairly close agreement at Mach numbers from 11 to 14.5 with the distribution predicted by the theory of Stine and Wanlass (NACA Technical Note 3344).

The experimental heating rates on the conical section of the nose were very much below theoretical flat-plate turbulent magnitude and were in good agreement with laminar-cone theory with Reynolds number based on surface length from the stagnation point, the assumption of theoretical sharp-cone static pressure on the conical section being used.

Langley Aeronautical Laboratory,
National Advisory Committee for Aeronautics,
Langley Field, Va., Nov. 19, 1957.

REFERENCES

1. Stoney, William E., Jr., and Swanson, Andrew G.: Heat Transfer Measured on a Flat-Face Cylinder in Free Flight at Mach Numbers Up to 13.9. NACA RM L57E13, 1957.

2. Bland, William M., Jr., Swanson, Andrew G., and Kolenkiewicz, Ronald: Free-Flight Aerodynamic-Heating Data at Mach Numbers Up to 10.9 on a Flat-Faced Cylinder. NACA RM L57K29, 1957.

3. Bland, Wiliiam M., Jr., Rumsey, Charles B., Lee, Dorothy B., and Kolenkiewicz, Ronald: Free-Flight Aerodynamic-Heating Data to a Mach Number of 15.5 on a Blunted Conical Nose With a Total Angle of 29°. NACA RM L57F28, 1957.

4. Hill, P. R.: A Method of Computing the Transient Temperature of Thick Walls From Arbitrary Variation of Adiabatic-Wall Temperature and Heat Transfer Coefficient. NACA TN 4105, 1957.

5. Fay, J. A., and Riddell, F. R.: Theory of Stagnation Point Heat Transfer in Dissociated Air. Res. Rep. 1, AVCO Res. Lab., June 1956 (rev. Apr. 1957). (Formerly AVCO Res. Note 18.)

6. Ames Research Staff: Equations, Tables, and Charts for Compressible Flow. NACA Rep. 1135, 1953. (Supersedes NACA TN 1428.)

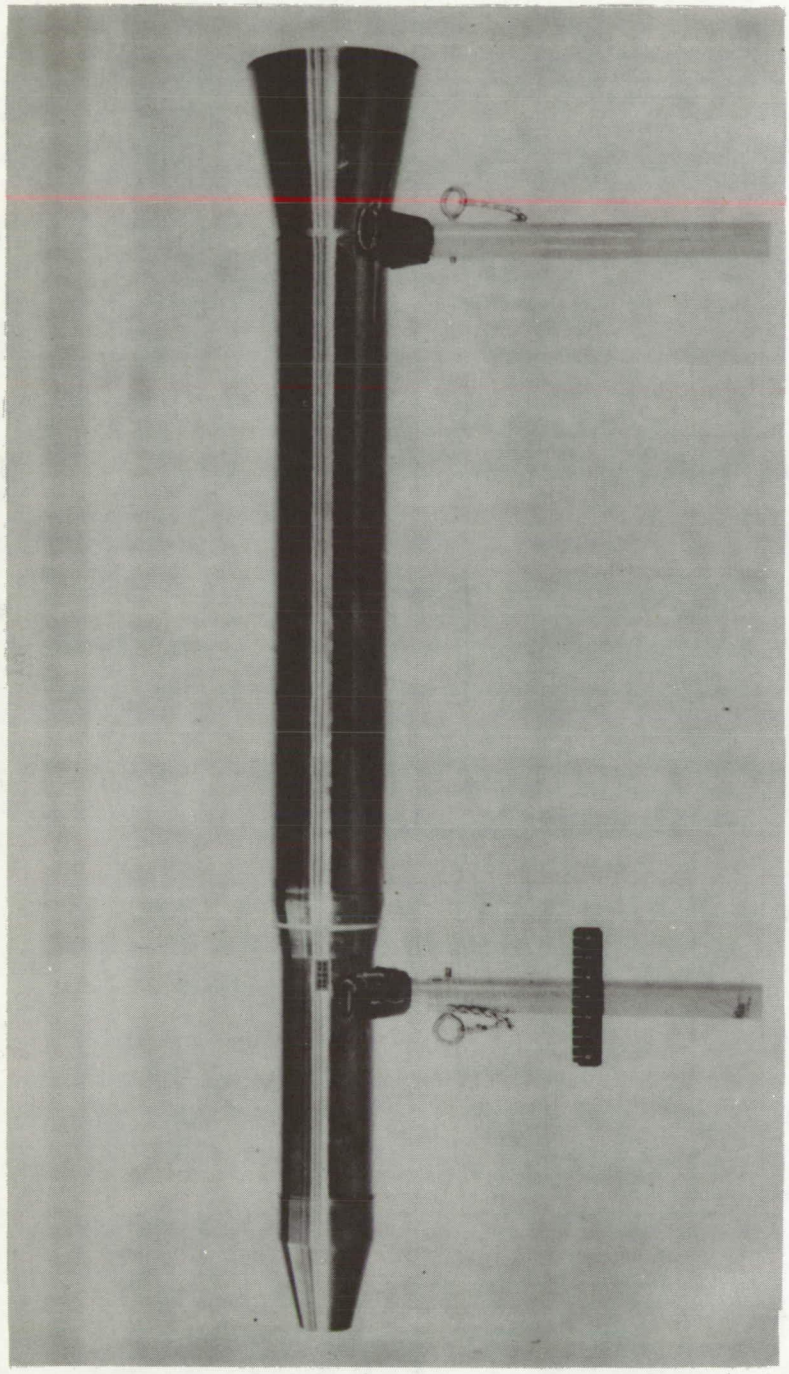
7. Stine, Howard A., and Wanlass, Kent: Theoretical and Experimental Investigation of Aerodynamic-Heating and Isothermal Heat-Transfer Parameters on a Hemispherical Nose With Laminar Boundary Layer at Supersonic Mach Numbers. NACA TN 3344, 1954.

8. Lees, Lester: Laminar Heat Transfer Over Blunt-Nosed Bodies at Hypersonic Flight Speeds. Jet Propulsion, vol. 26, no. 4, Apr. 1956, pp. 259-269.

9. Van Driest, E. R.: The Problem of Aerodynamic Heating. Aero. Eng. Rev., vol. 15, no. 10, Oct. 1956, pp. 26-41.

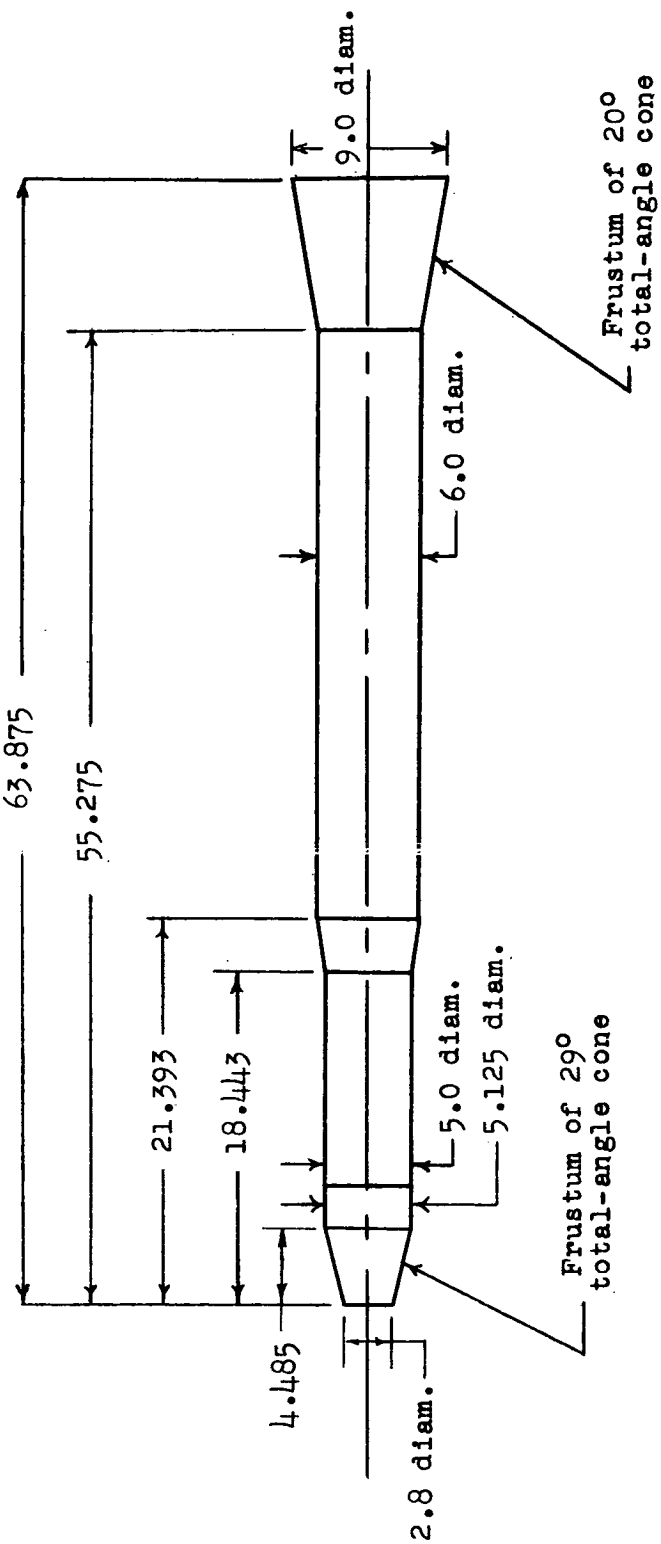
TABLE I.- FAIRED INSIDE WALL TEMPERATURES

Time, sec	Temperature, °F, at station -															
	1	2	3_a	3_b	3_c	4	5	6	7	8	9	10_a	10_b	11	12	13
99.0	178	178	175	179	181	180	179	175	176	173	172	168	168	166	166	165
99.2	179	179	177	180	182	180	180	175	176	173	172	168	168	167	167	165
99.4	180	180	178	181	183	181	180	175	176	174	173	169	168	167	167	166
99.6	182	181	180	182	184	182	181	175	177	175	173	170	169	168	167	167
99.8	185	183	183	184	185	184	182	175	178	175	174	170	170	168	168	167
100.0	188	185	185	186	187	185	183	176	179	176	175	171	170	169	168	167
100.2	190	188	187	189	188	187	185	177	180	177	176	172	170	170	169	168
100.4	192	190	190	192	190	189	186	179	182	179	177	173	171	171	170	168
100.6	194	192	194	195	192	192	187	181	183	180	178	173	172	172	170	168
100.8	197	195	198	198	194	194	189	183	185	182	179	174	173	174	171	168
101.0	200	198	200	201	196	196	191	185	186	184	180	175	174	175	172	169
101.2	203	202	205	204	199	199	193	189	187	186	182	177	175	177	174	170
101.4	207	206	208	208	202	201	195	192	189	189	184	178	177	180	175	170
101.6	210	210	212	211	205	205	198	195	191	191	186	179	178	182	177	171
101.8	214	214	217	216	210	207	200	199	193	195	188	181	180	185	179	172
102.0	220	218	220	222	215	211	202	203	195	198	190	182	182	188	181	174
102.2	227	223	225	229	222	216	205	207	197	203	193	184	185	192	184	175
102.4	237	229	232	238	231	225	209	211	200	208	196	187	187	196	187	177
102.6	248	239	241	250	242	235	214	215	205	215	202	192	190	201	191	179
102.8	263	252	254	263	259	250	222	220	211	221	210	199	194	207	195	180
103.0	278	268	272	280	279	267	232	227	218	229	220	210	200	214	200	183
103.2	299	290	296	300	305	289	244	239	227	239	232	223	207	221	208	185
103.4	324	319	326	327	335	317	261	255	239	251	247	238	218	230	215	190
103.6	361	358	367	367	375	353	285	275	256	267	265	255	231	241	223	195
103.8	408	406	415	424	426	408	322	295	285	289	287	276	249	253	232	204
104.0	464	465	475	490	494	473	364	327	320	316	312	299	271	269	245	214
104.2	533	533	546	561	574	541	412	367	358	353	340	326	298	287	259	227
104.4	610	612	628	643	659	616	466	417	399	396	374	356	326	308	276	240
104.6	699	697	717	734	750	701	525	471	444	442	411	388	361	332	294	255
104.8	798	794	815	839	849	800	590	529	492	491	451	423	401	360	314	269
105.0	902	900	934	976	970	919	665	595	547	548	495	463	446	391	336	282
105.2	1,008	1,011	1,074	1,129	1,106	1,052	753	673	611	615	542	509	495	426	362	295
105.4	1,114	1,123	1,237	1,287	1,271	1,196	851	757	680	688	590	556	546	466	393	309



(a) Photograph of the model. L-57-1926.1

Figure 1.- Test model.



(b) Pertinent dimensions in inches of the model.

Figure 1.- Concluded.

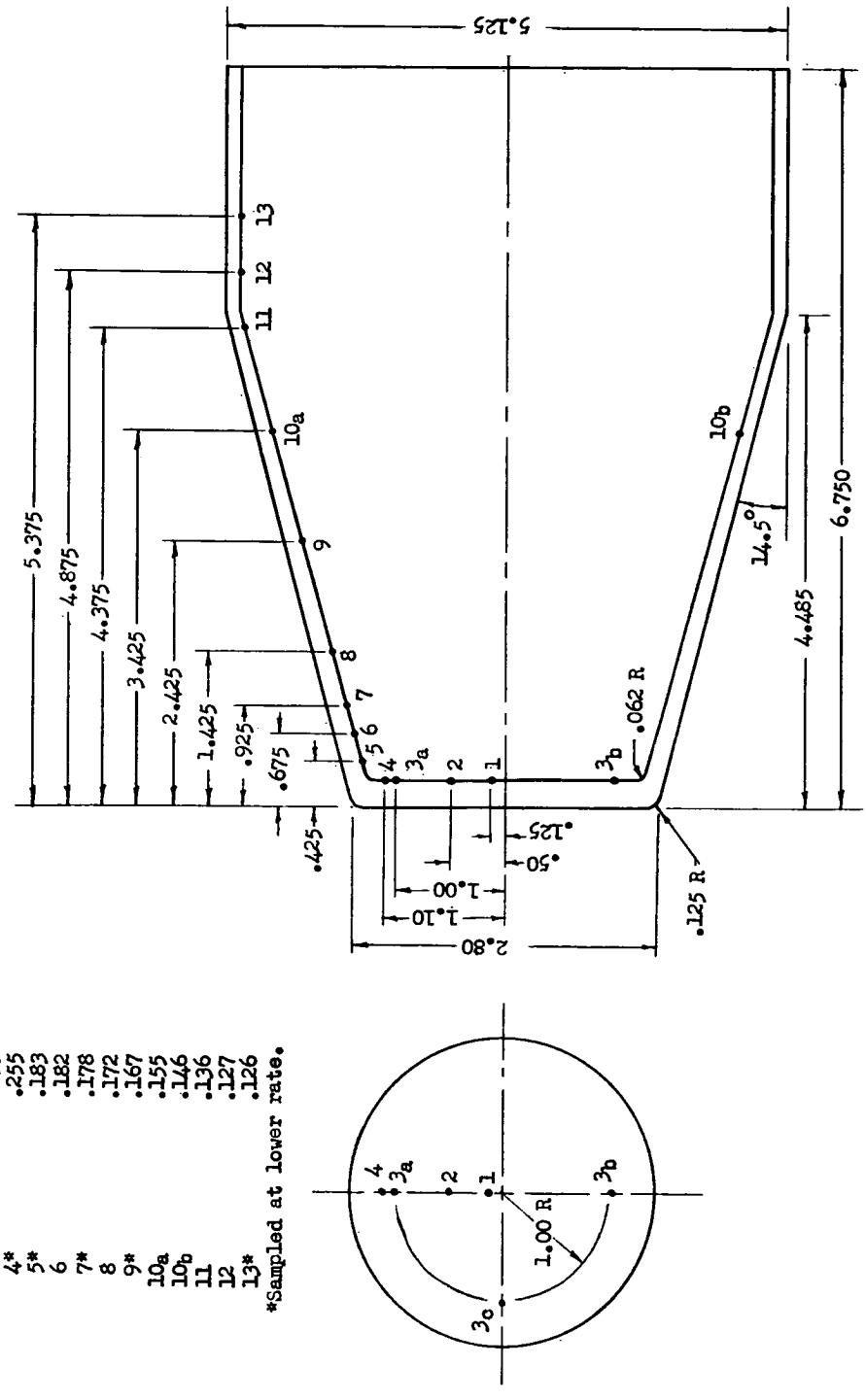


Figure 2.- Details of test nose and thermocouple locations.

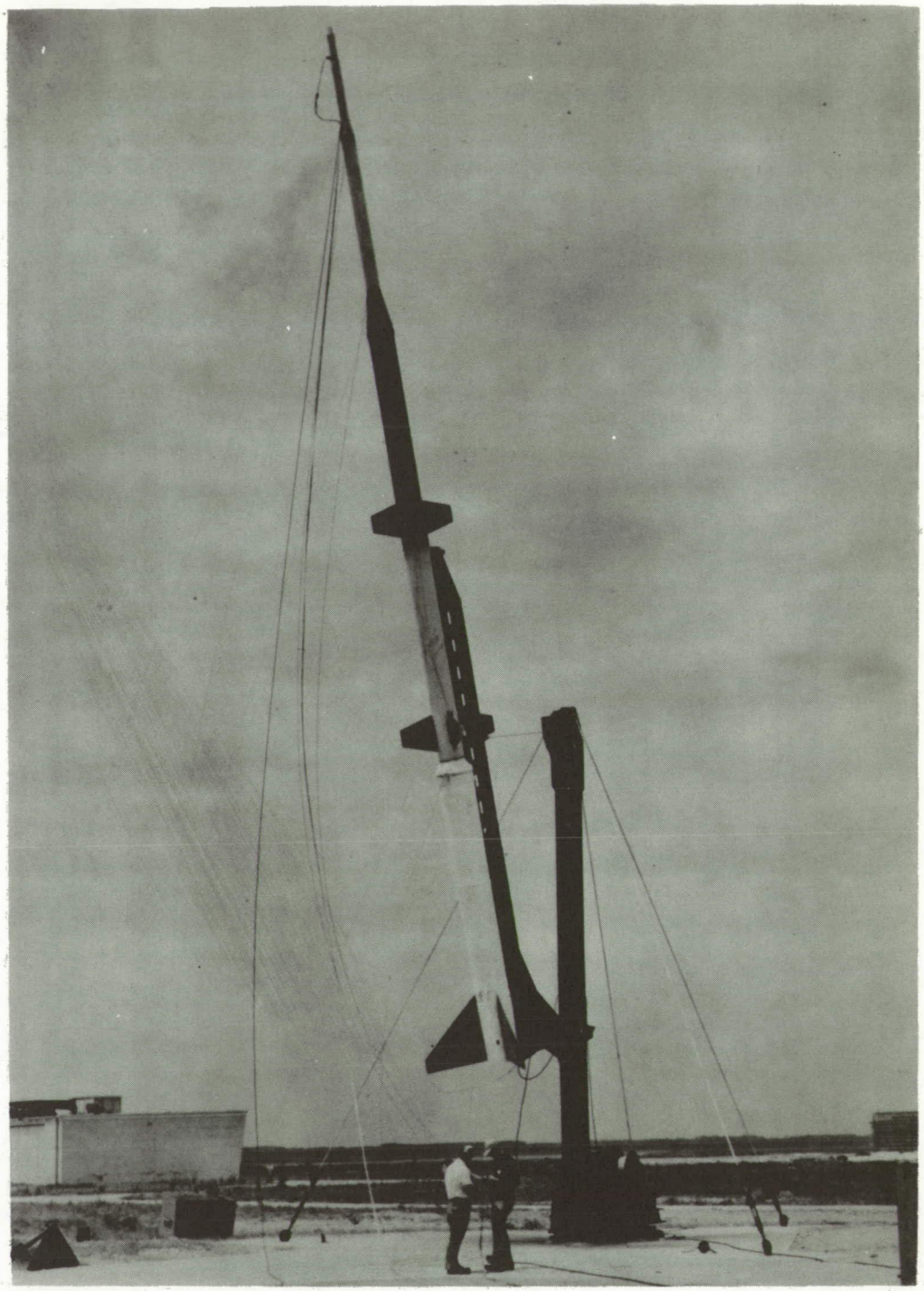


Figure 3.- Model and booster on launcher. L-57-2068

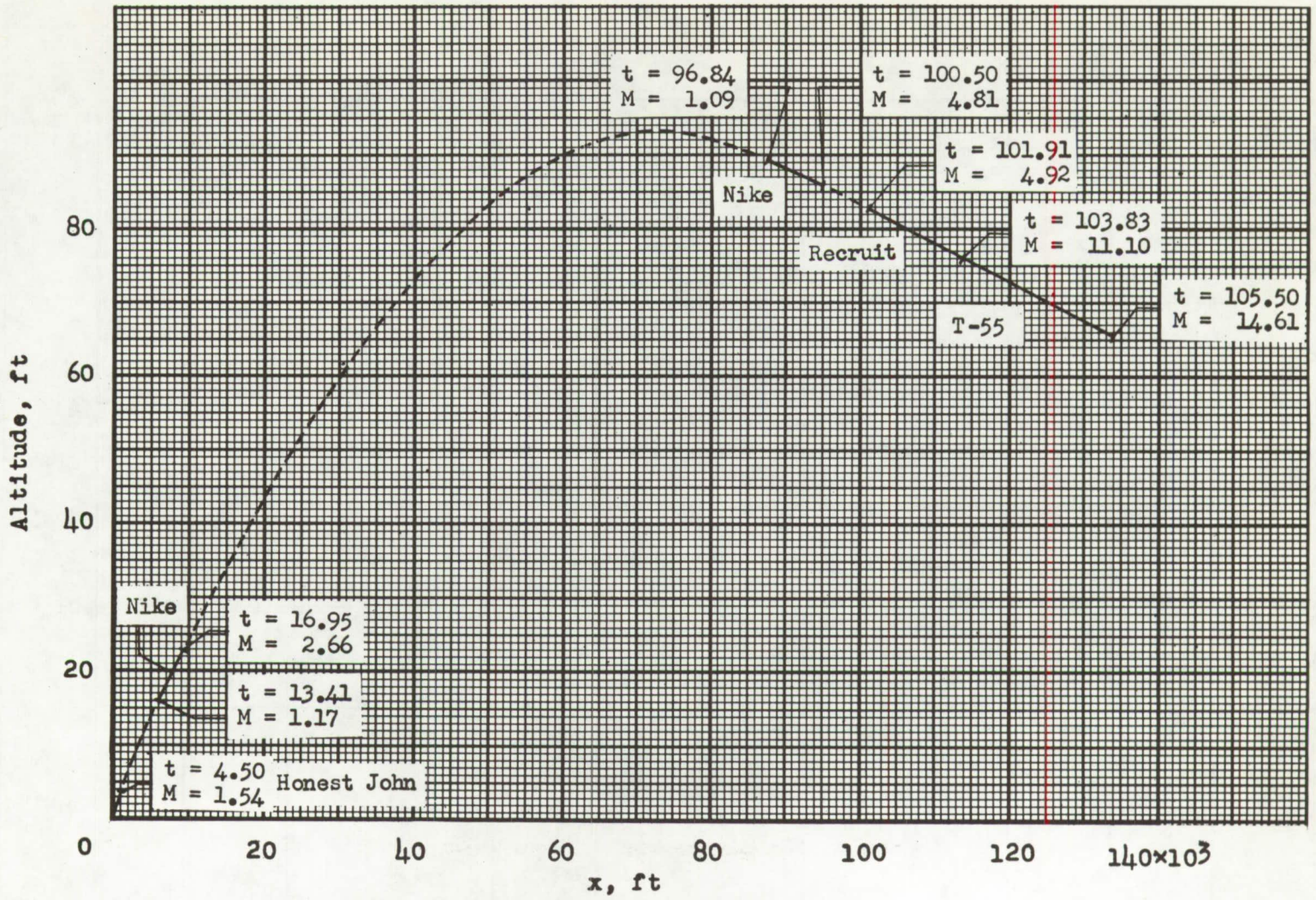


Figure 4.- Flight trajectory.

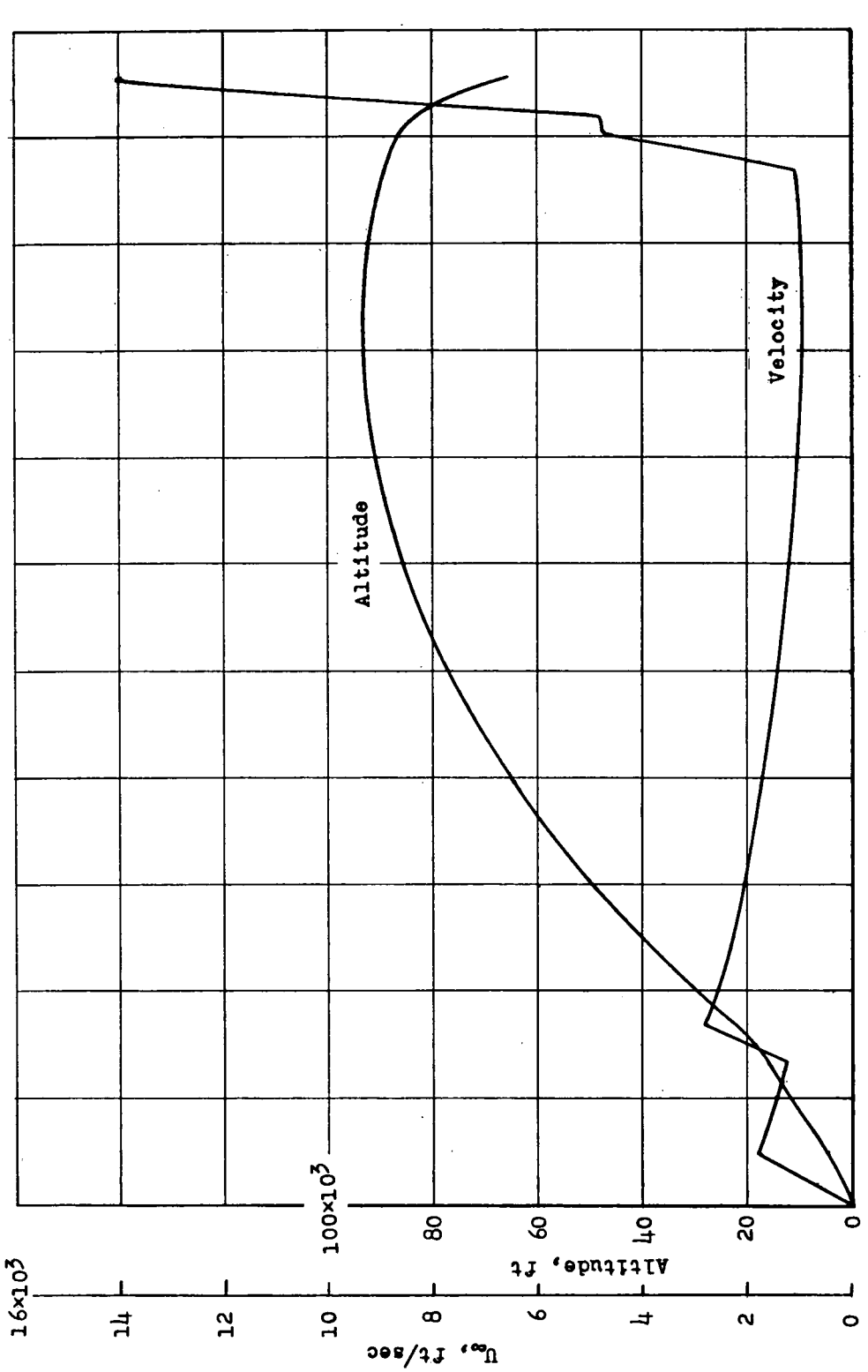
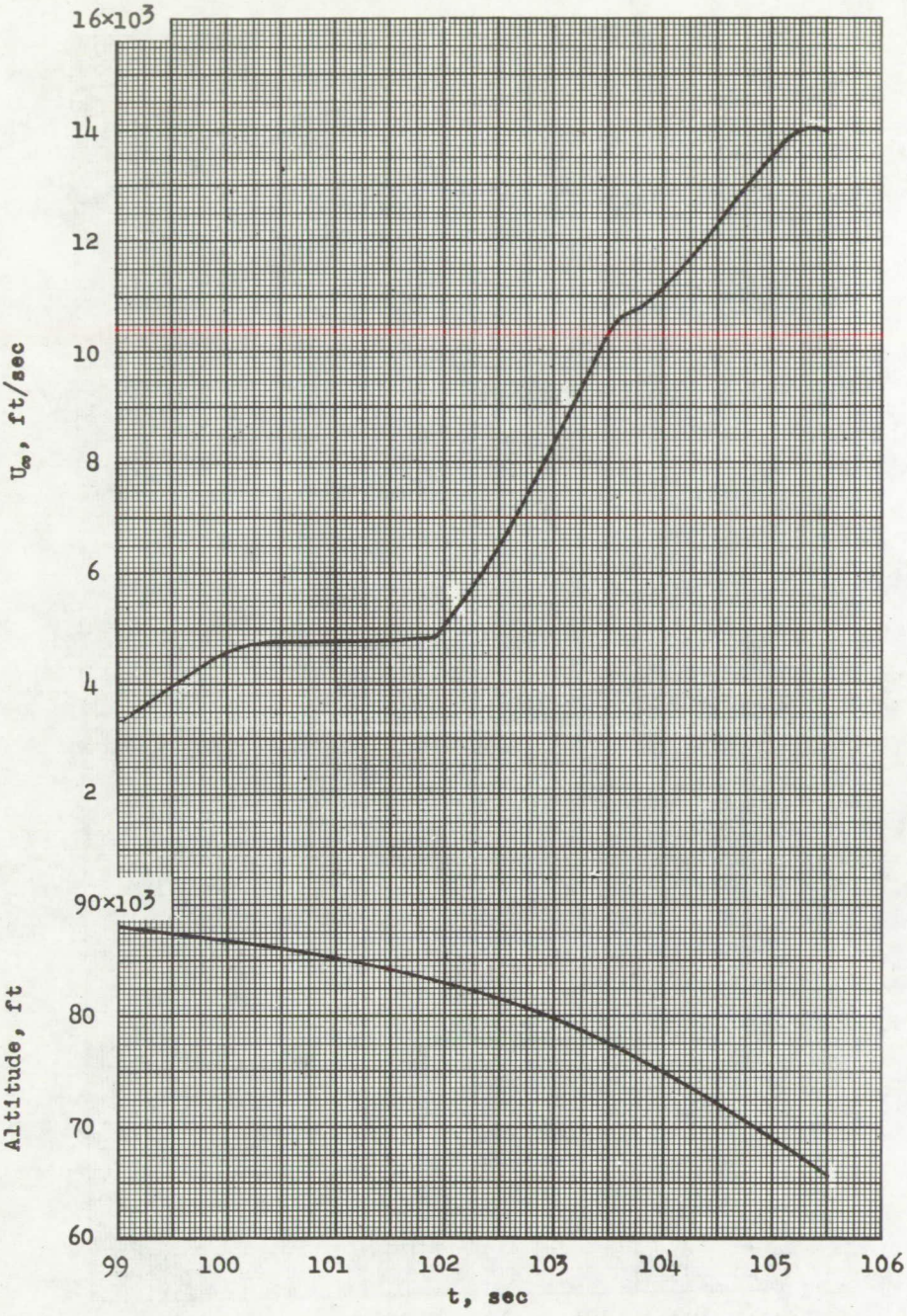
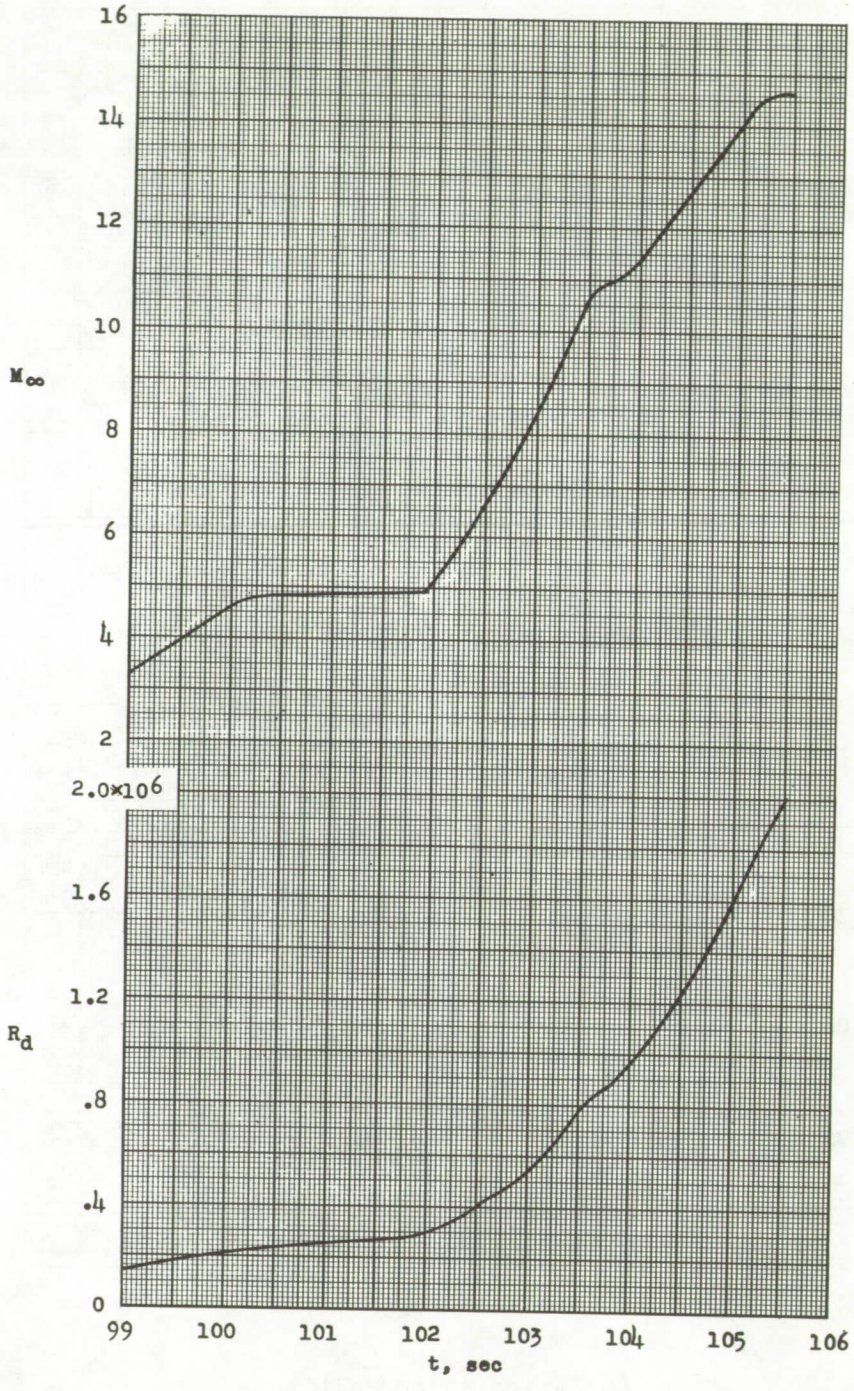


Figure 5.- Time histories of altitude and velocity.



(a) Velocity and altitude.

Figure 6.- Time histories of flight conditions during high-speed portion of test.



(b) Mach number and Reynolds number based on flat-face diameter.

Figure 6.- Concluded.

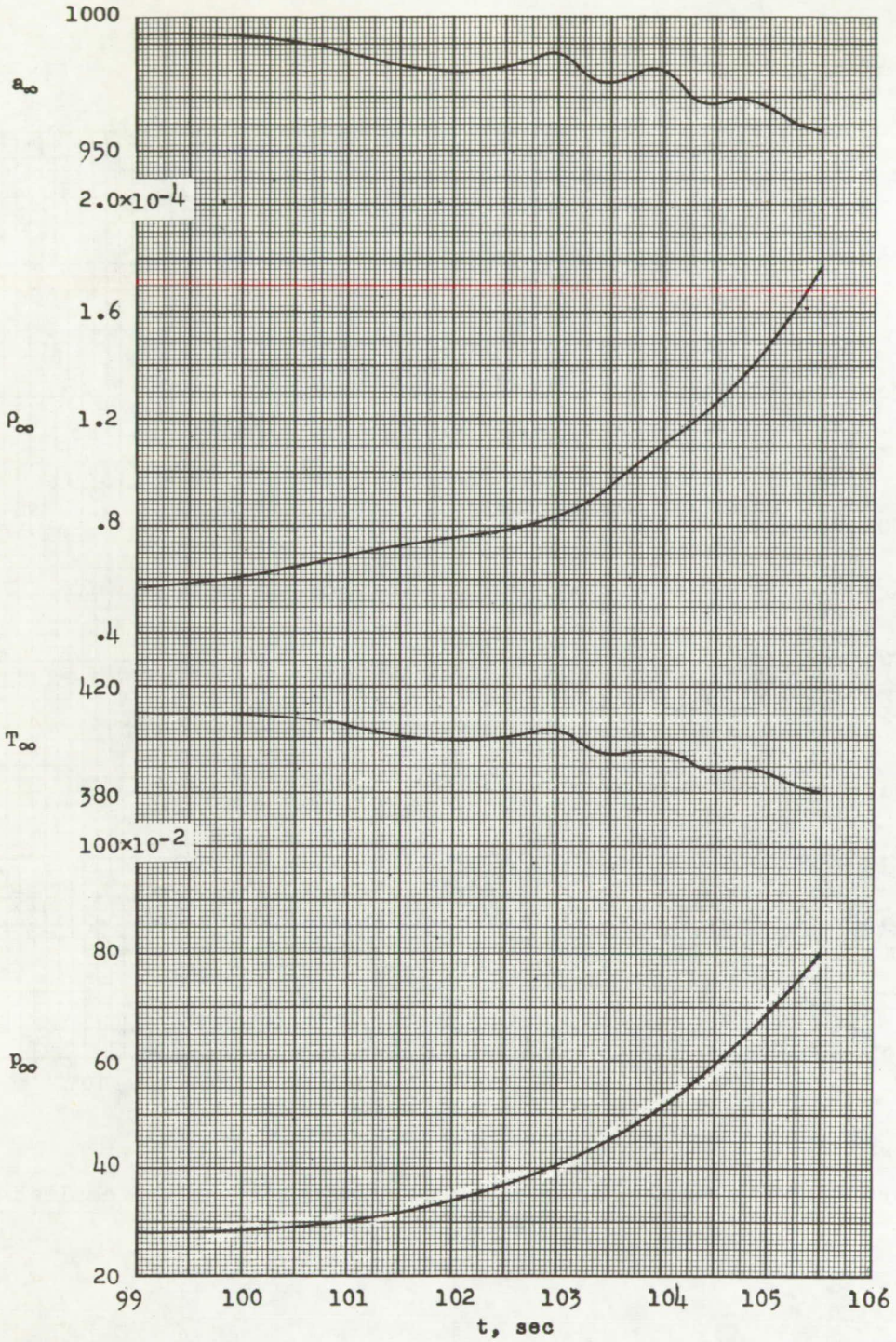


Figure 7.- Ambient conditions for high-speed portion of test.

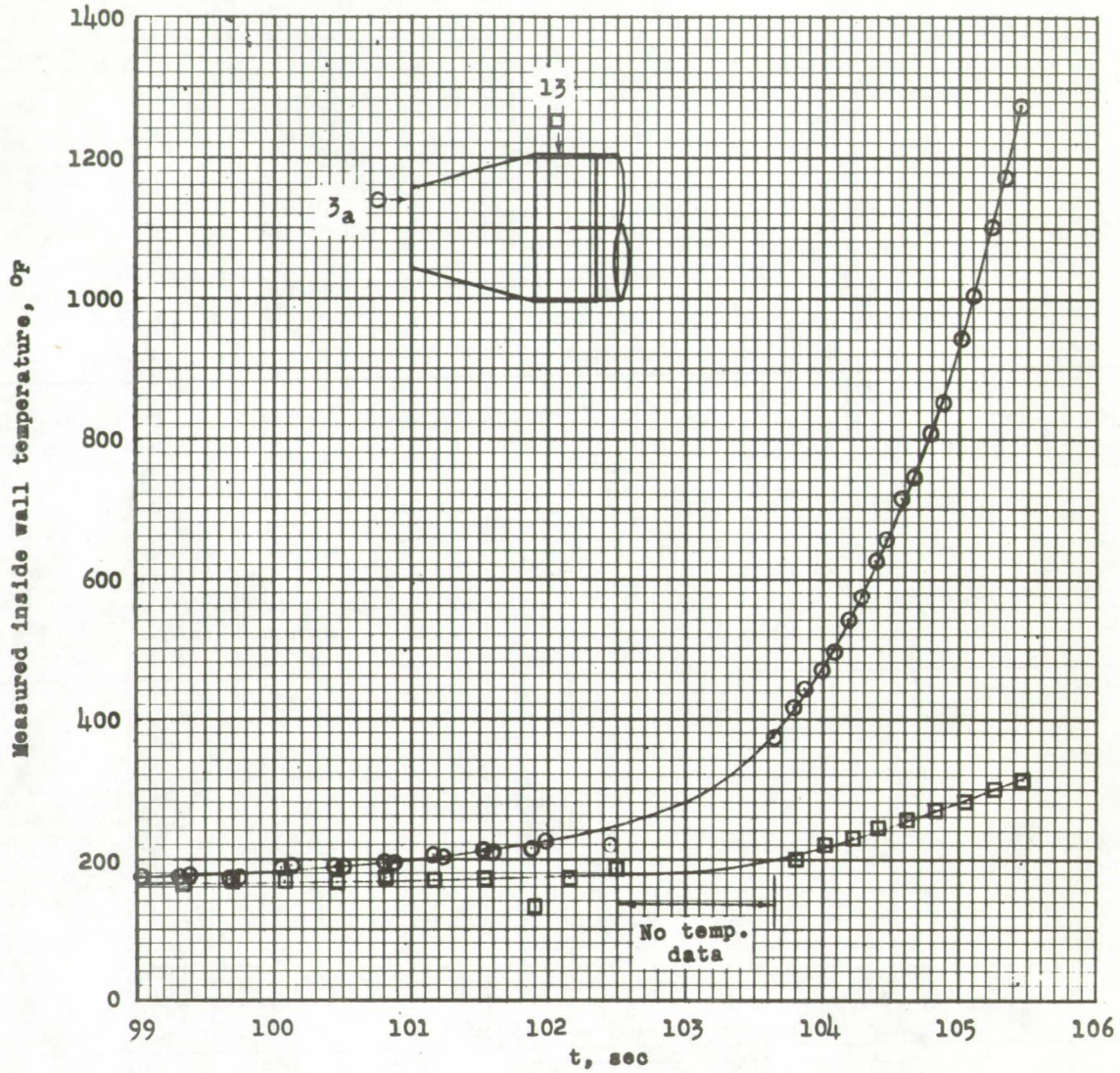


Figure 8.- Skin temperatures measured at the hottest and coolest measurement stations.

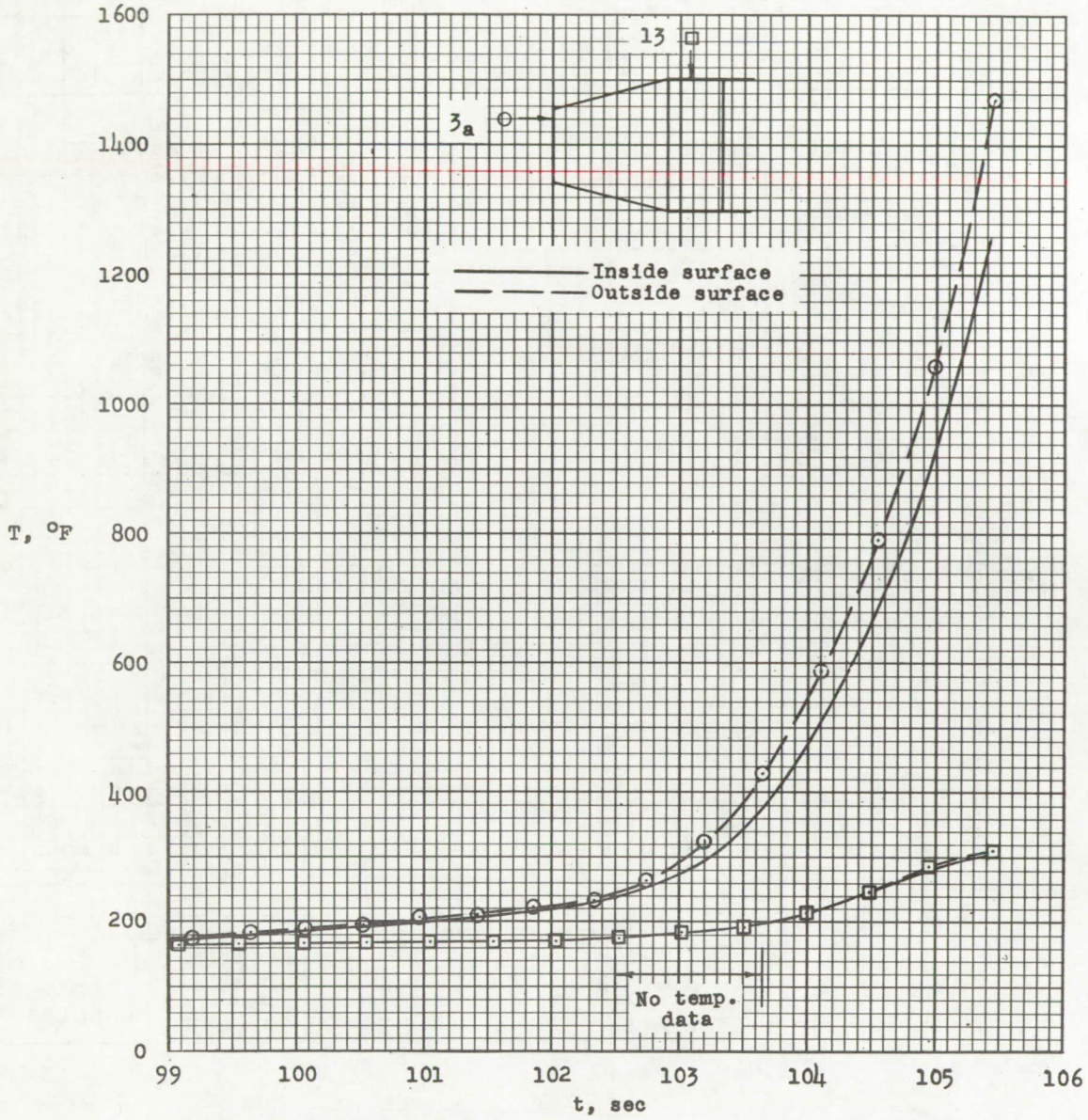


Figure 9.- Temperatures of outside skin surface computed from faired inside surface temperature measurement.

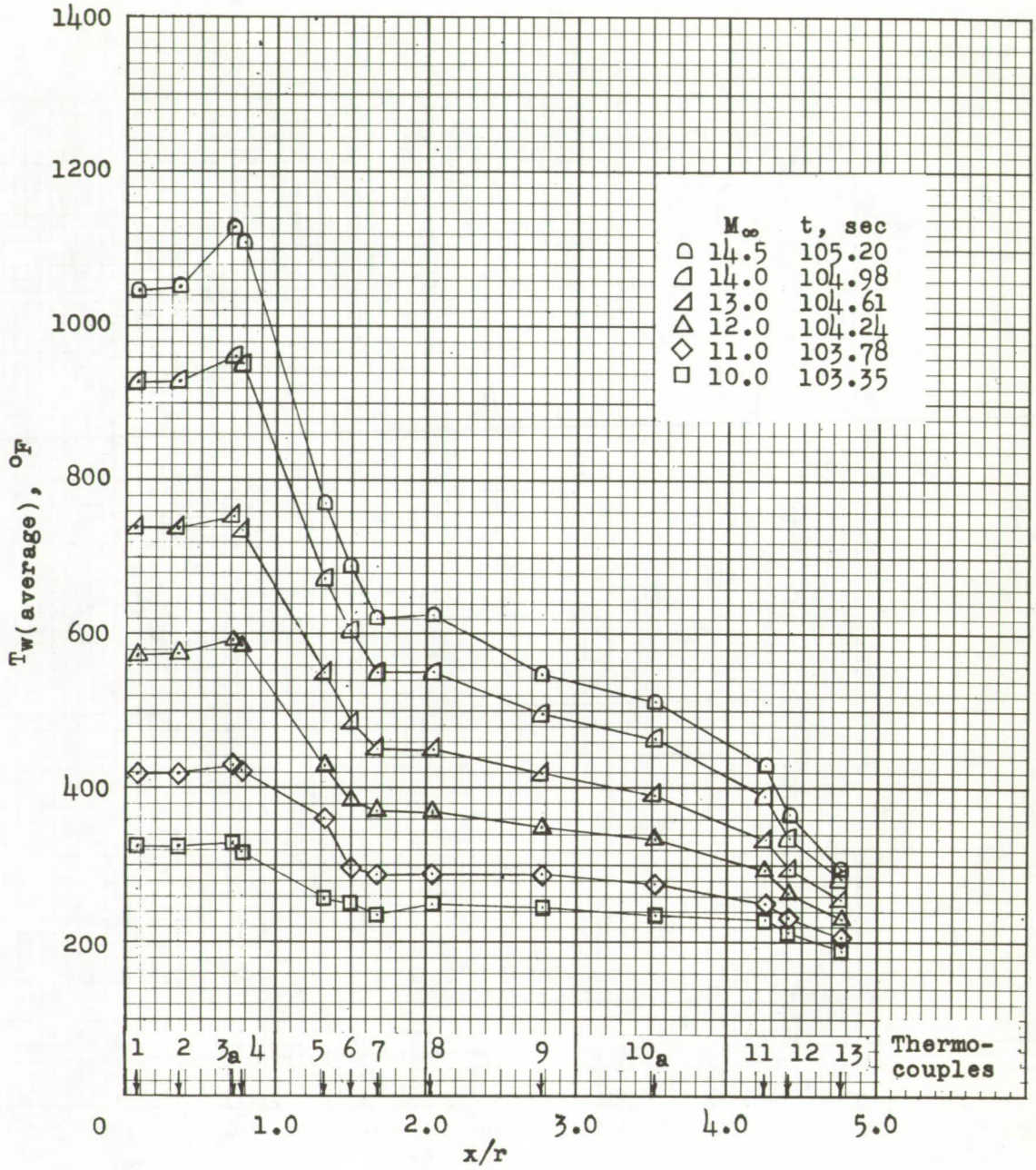
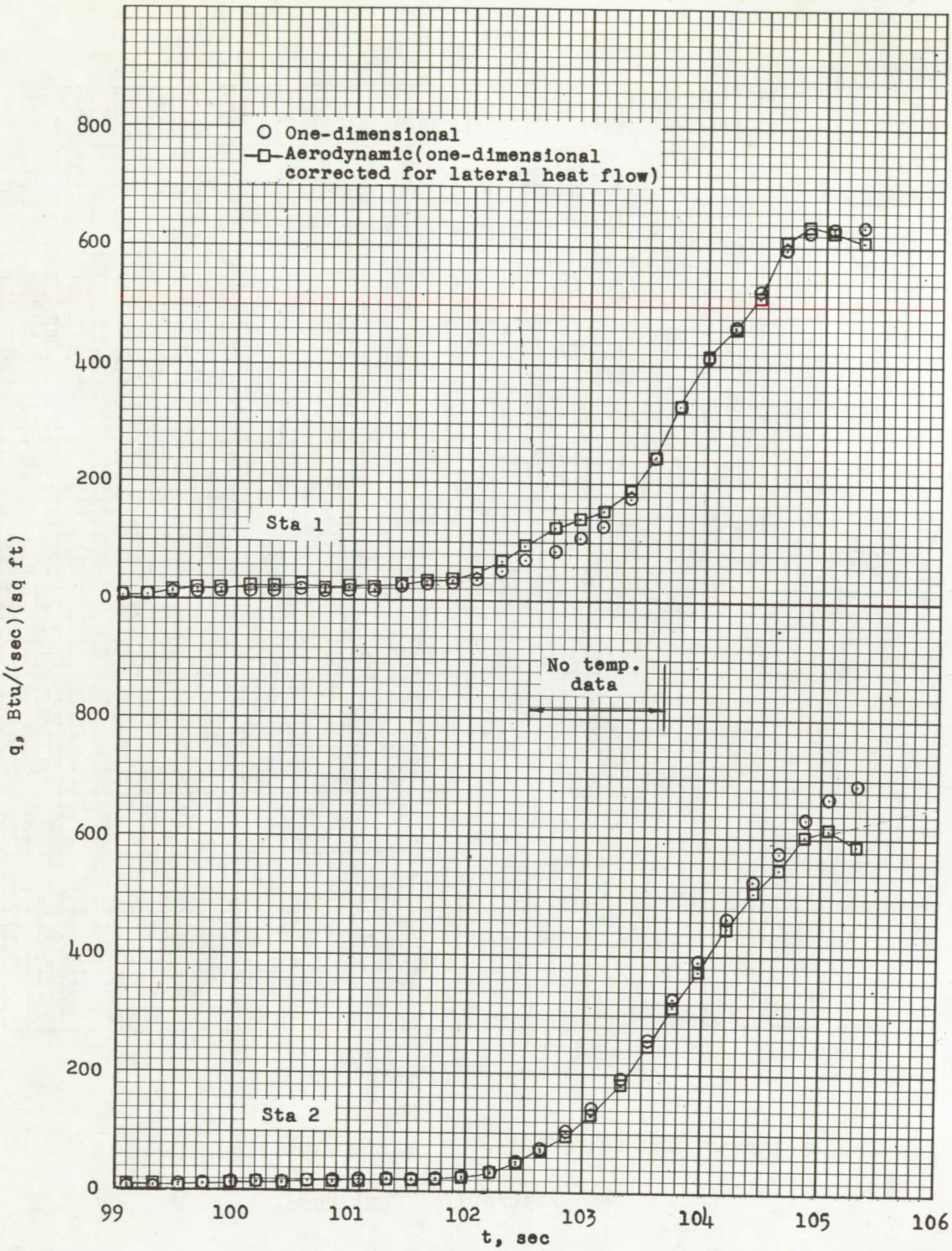
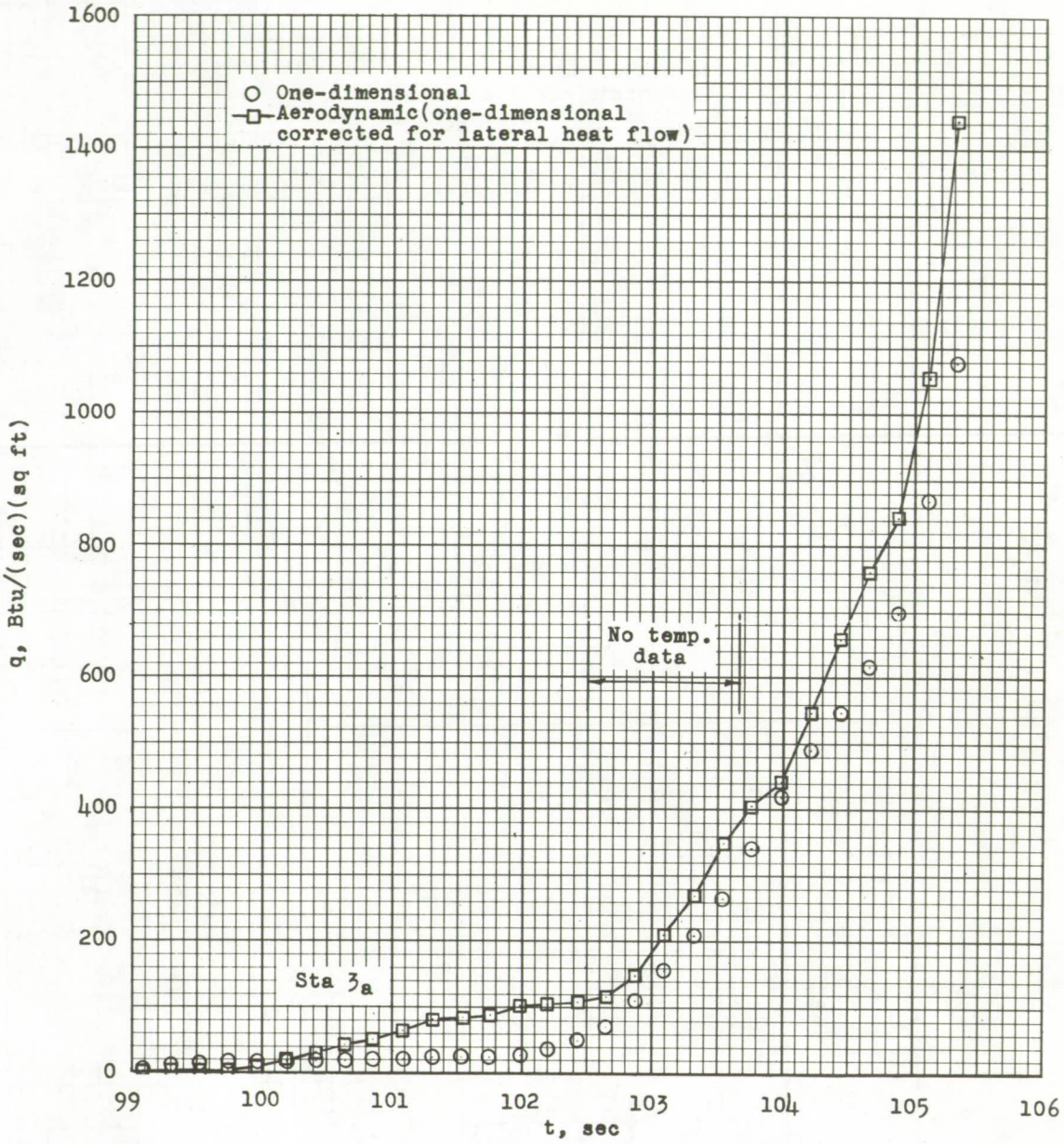


Figure 10.- Distributions of average wall temperature along nose surface at several times.



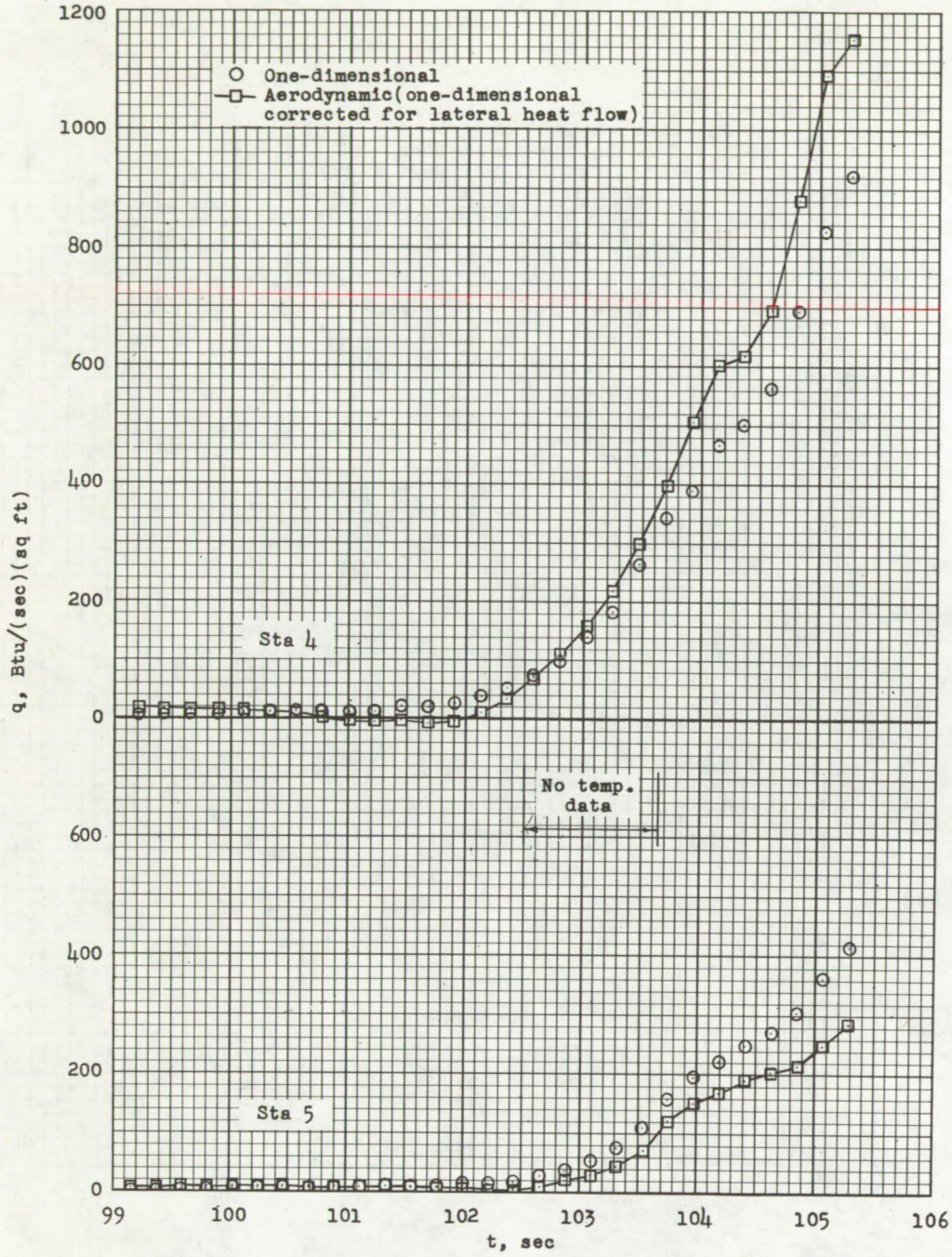
(a) Stations 1 and 2 on the flat face.

Figure 11.- Experimental heat-transfer data.



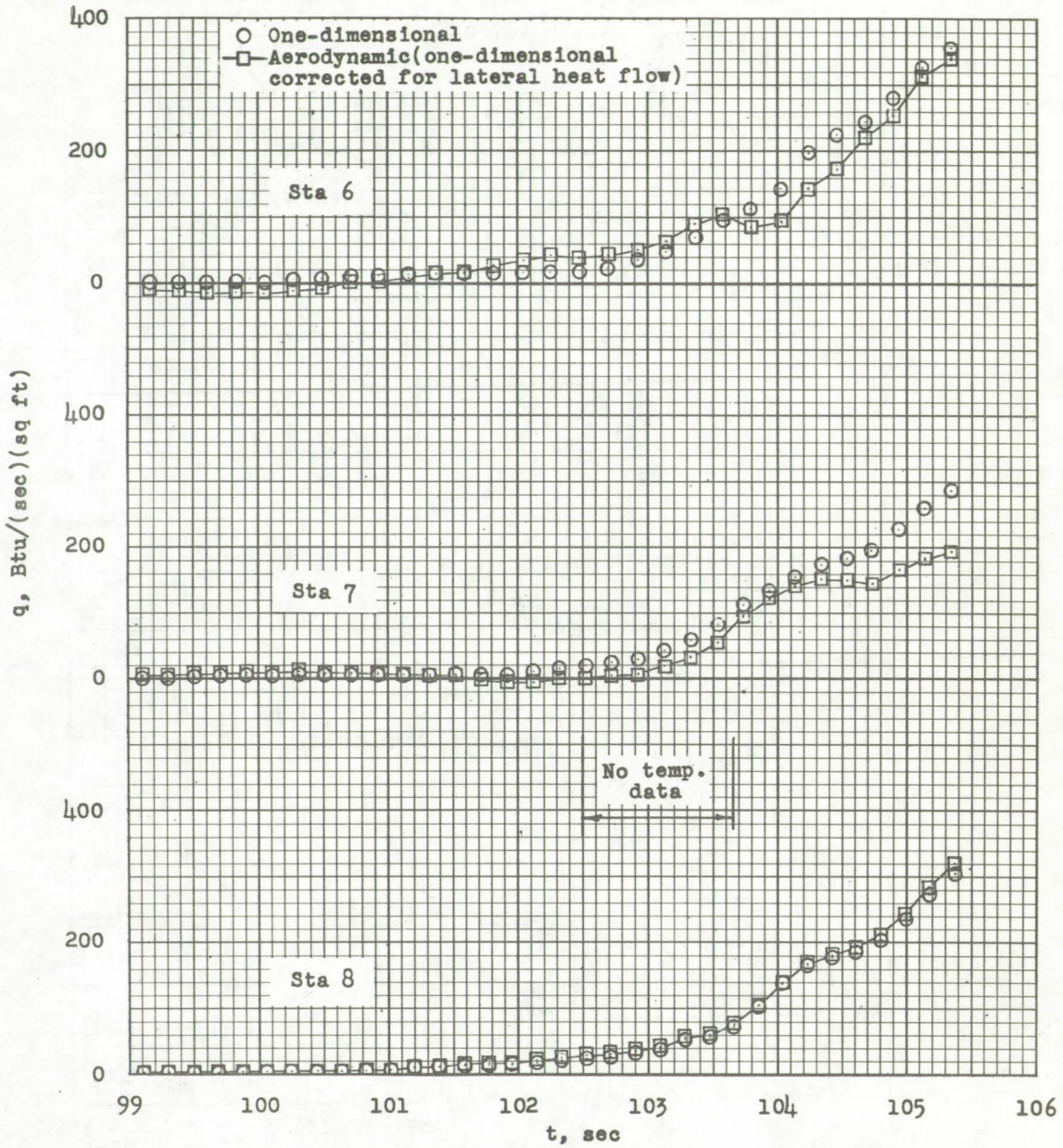
(b) Station 3a on the flat face.

Figure 11.- Continued.



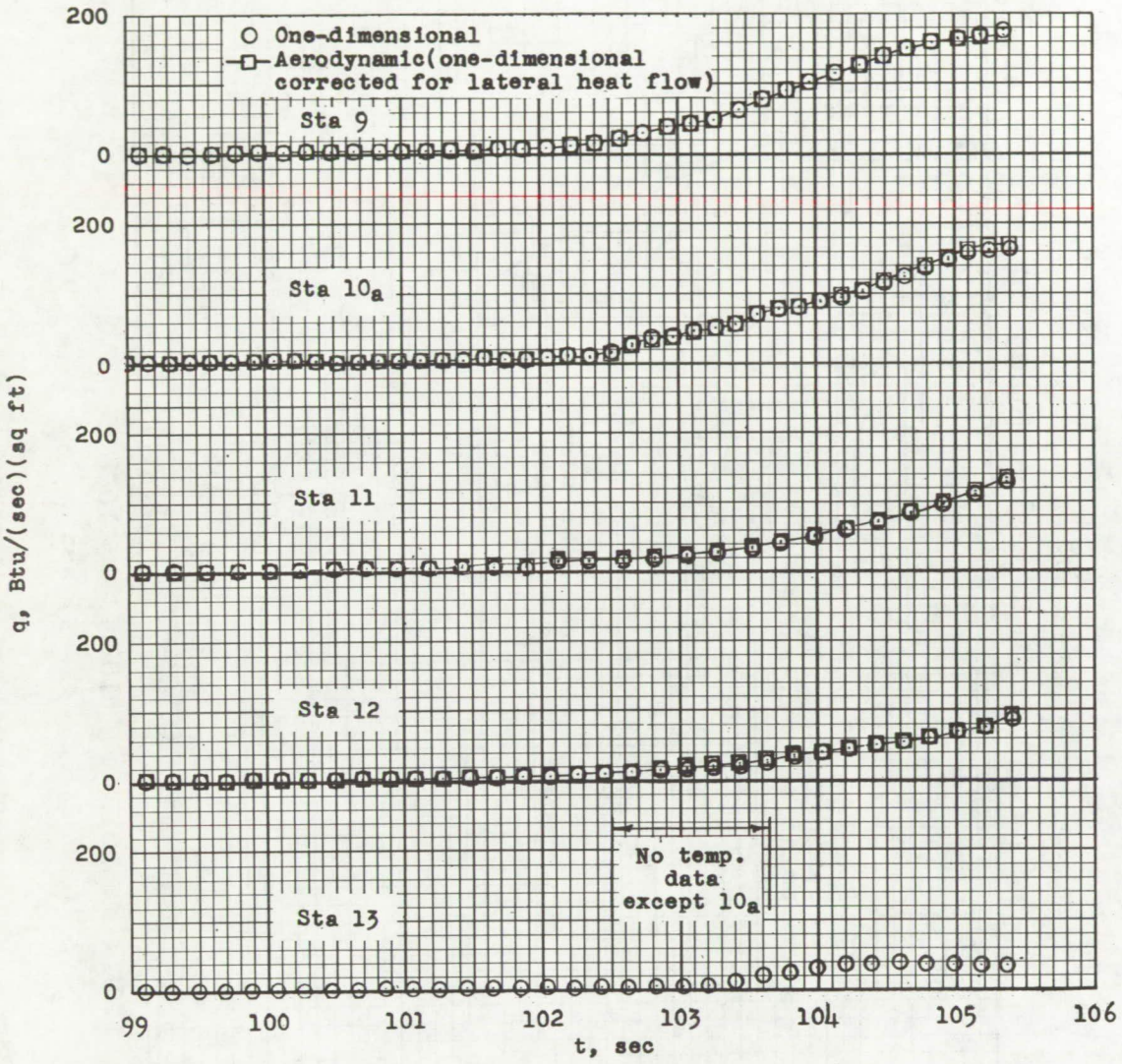
(c) Station 4 on the flat face and station 5 on the conical section.

Figure 11.- Continued.



(d) Stations 6, 7, and 8 on the conical section.

Figure 11.- Continued.



(e) Stations 9, 10a, and 11 on the conical section, and 12 and 13 on the cylinder.

Figure 11.- Concluded.

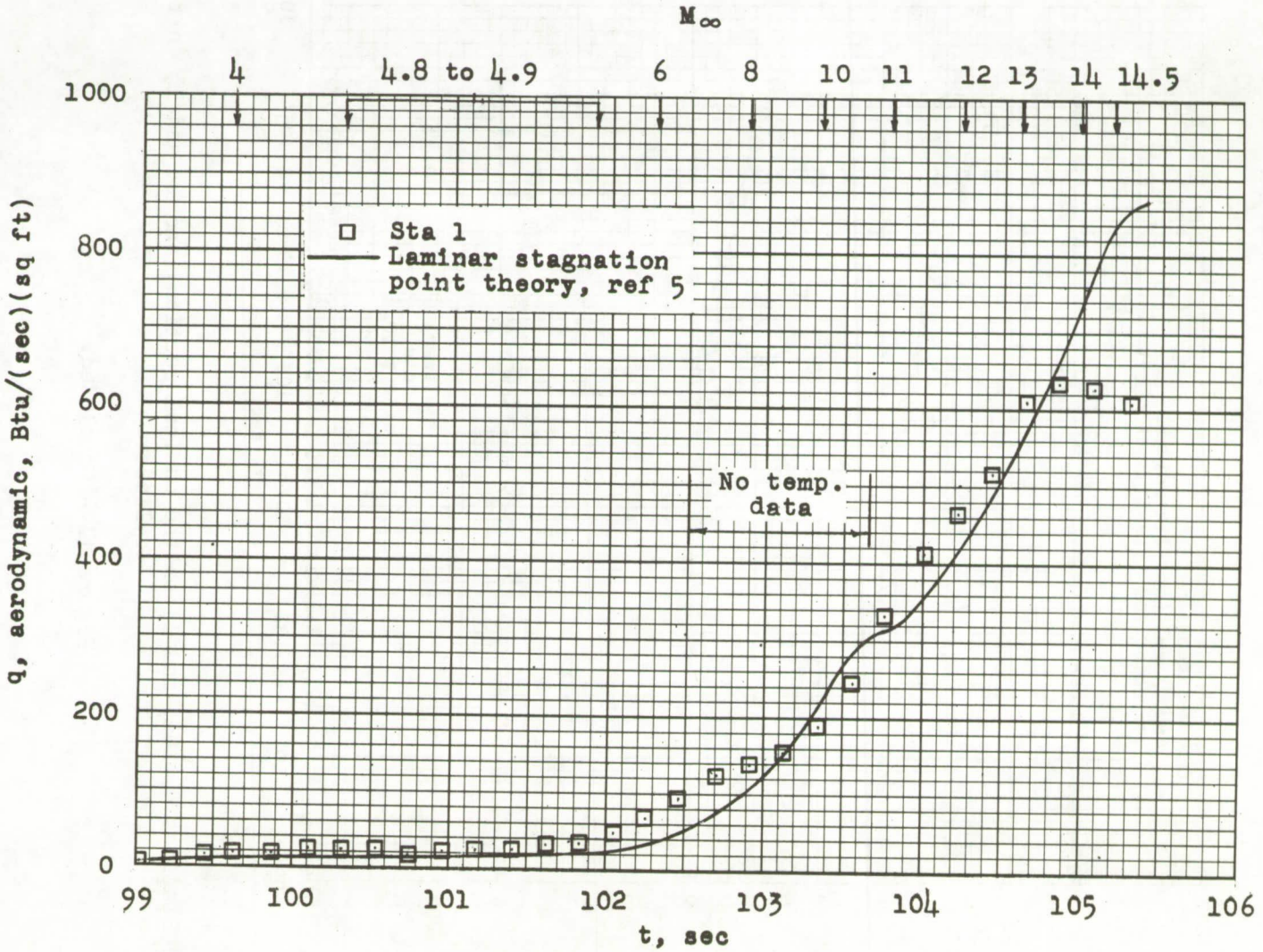


Figure 12.- Experimental and theoretical stagnation-point heating.

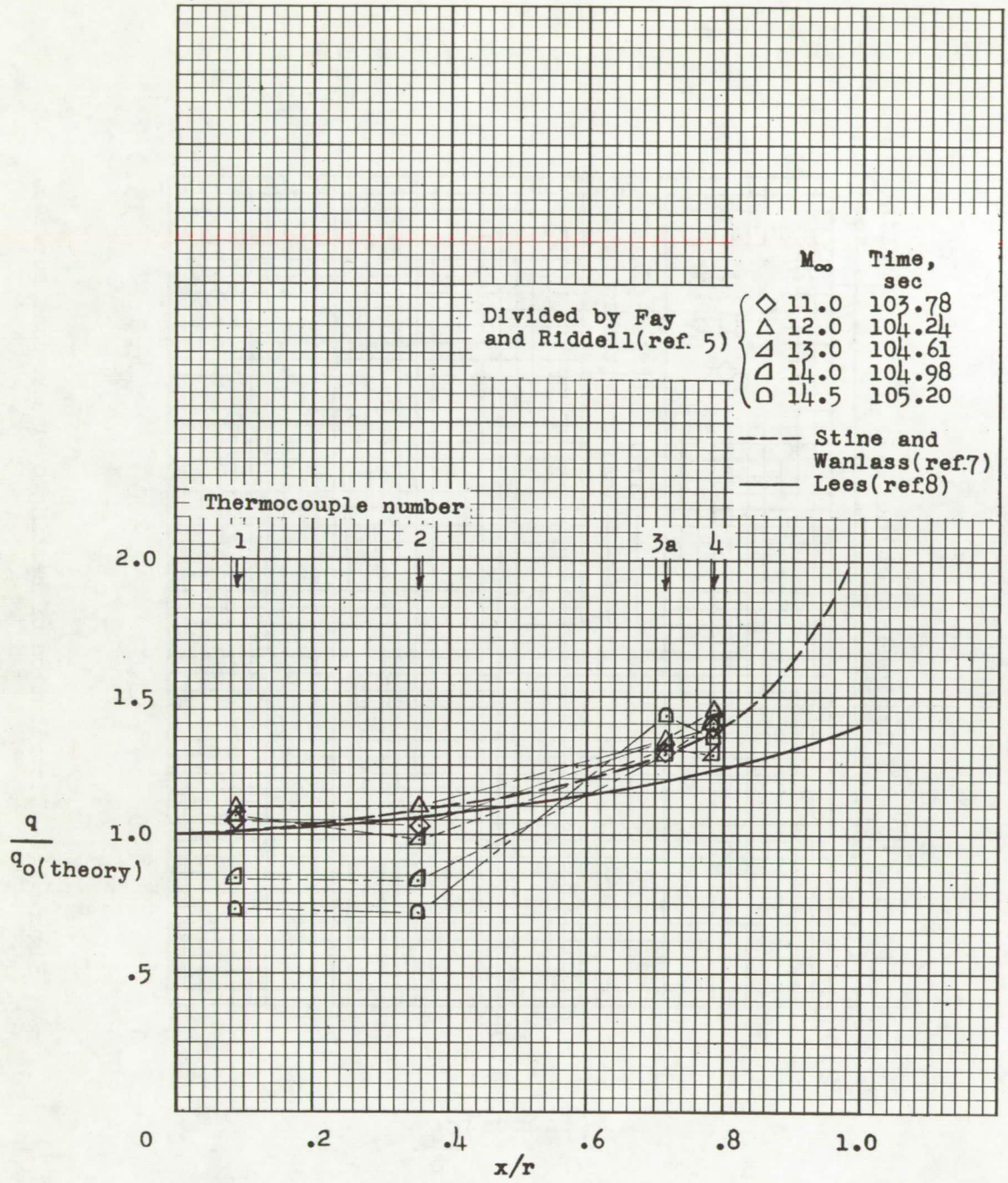


Figure 13.- Distribution of heat transfer across the flat face in terms of theoretical stagnation-point rates.

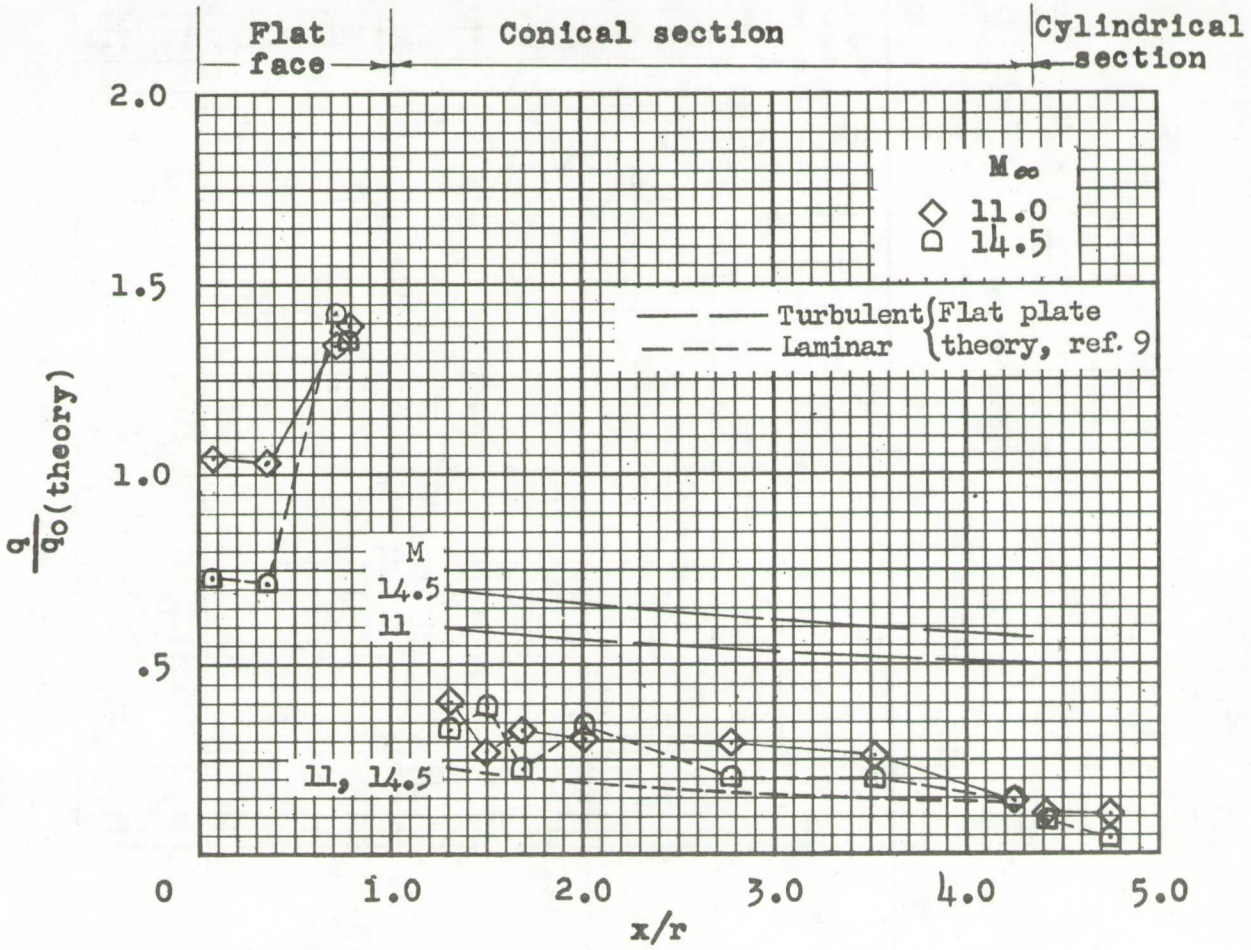
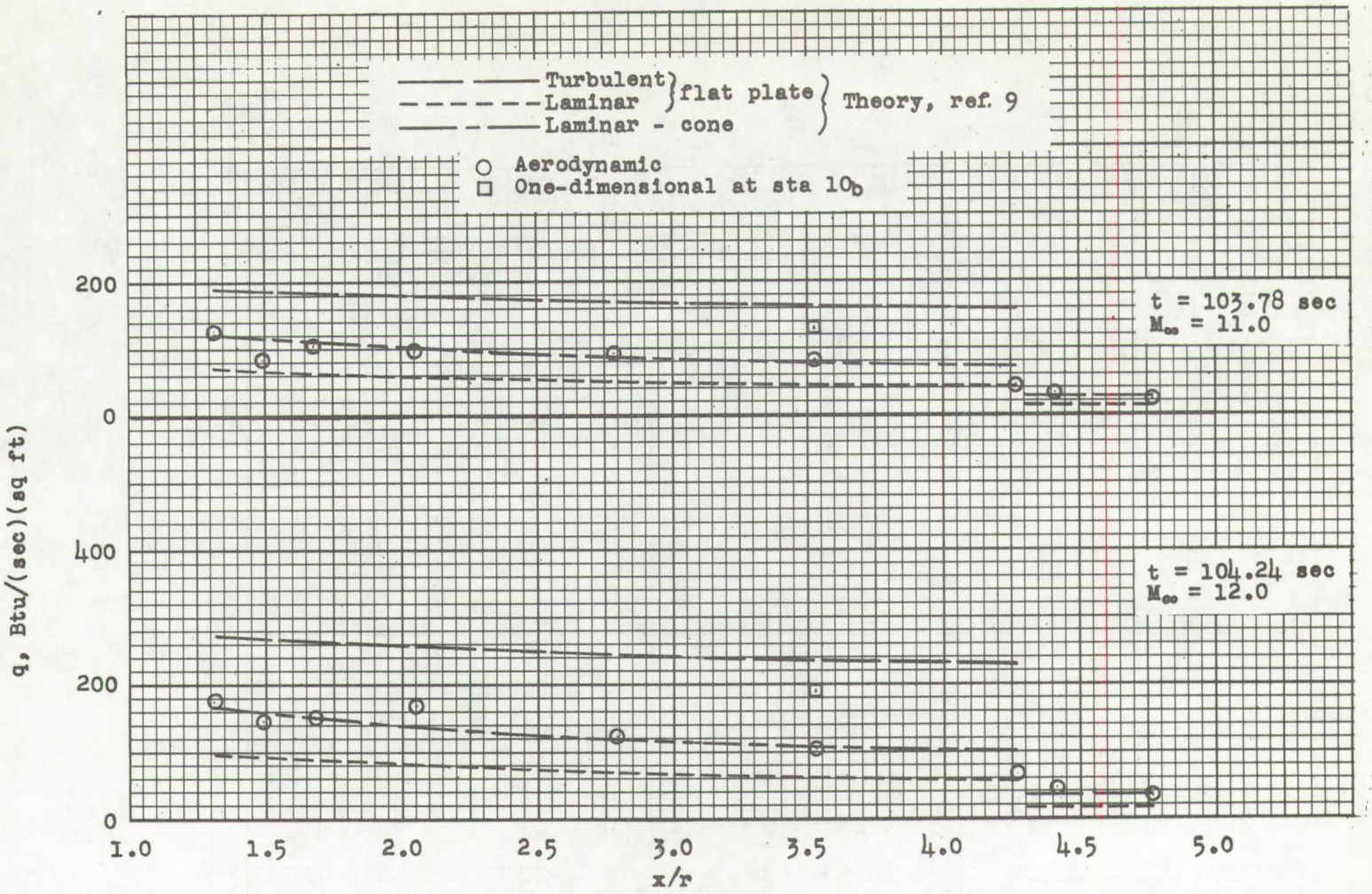
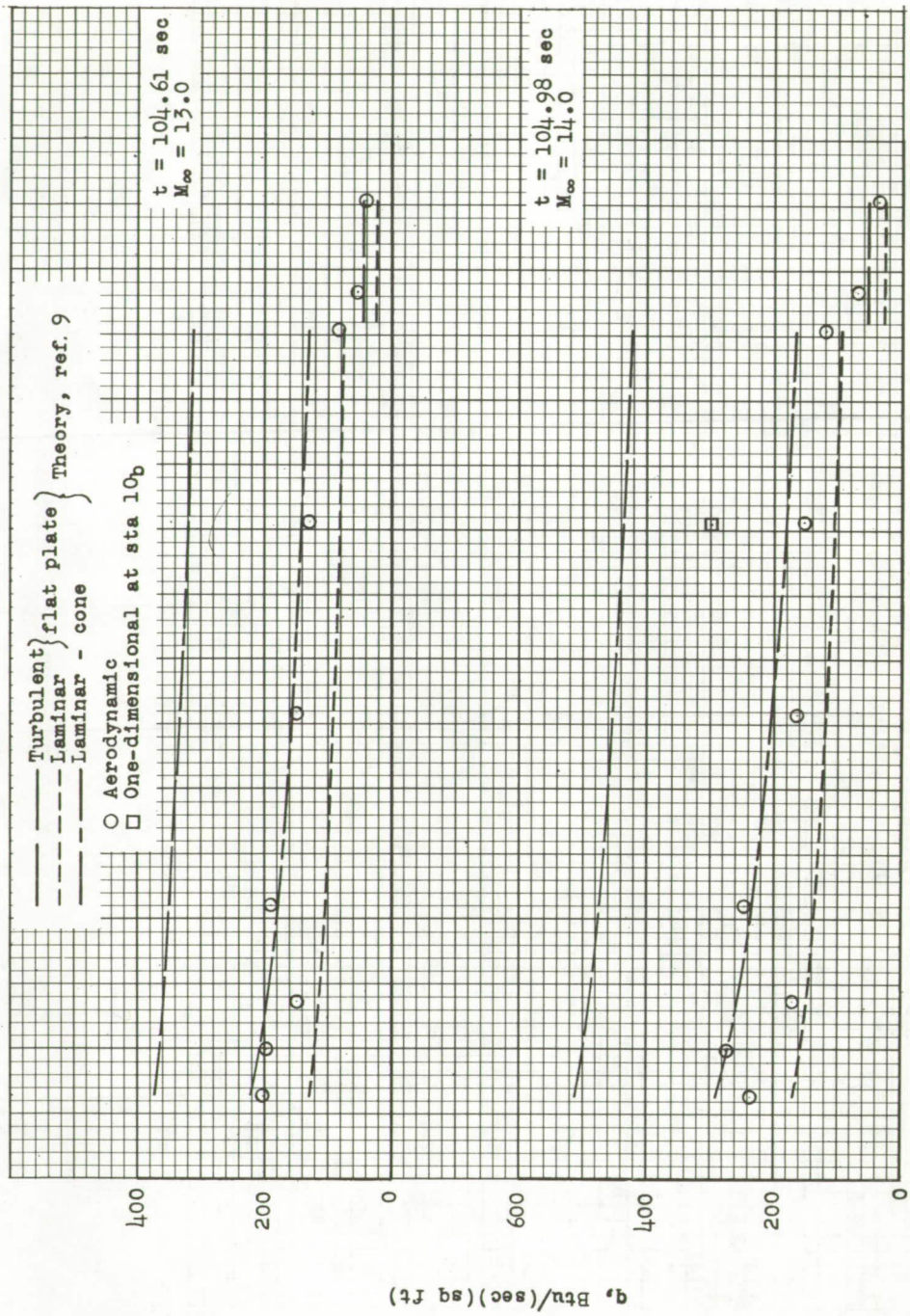


Figure 14.- Distribution of heating over the nose surface.



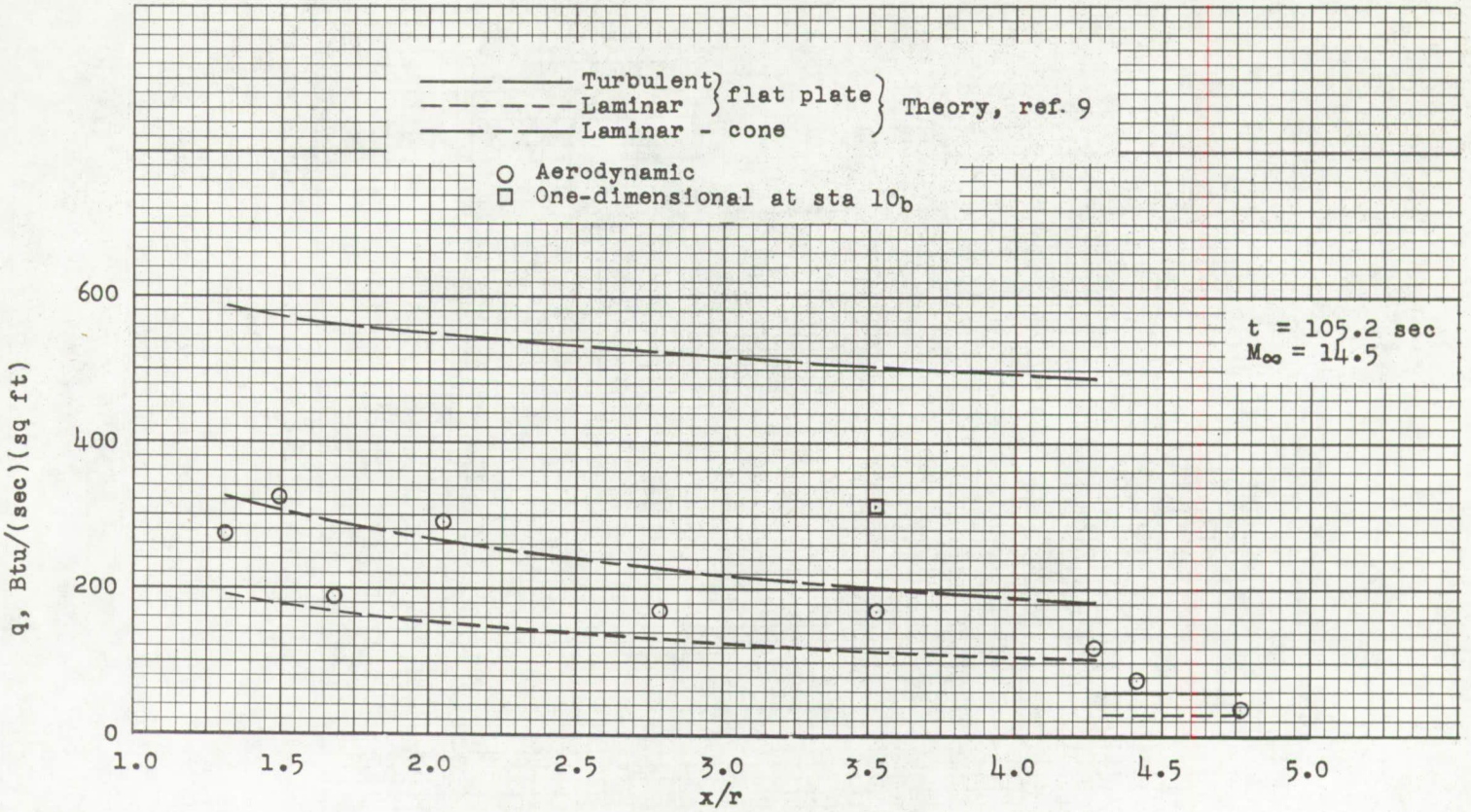
(a) Mach numbers of 11 and 12.

Figure 15.- Experimental and theoretical heating on the conical and spherical sections of the nose.



(b) Mach numbers of 13 and 14.

Figure 15.- Continued.



(c) Mach number of 14.5.

Figure 15.- Concluded.

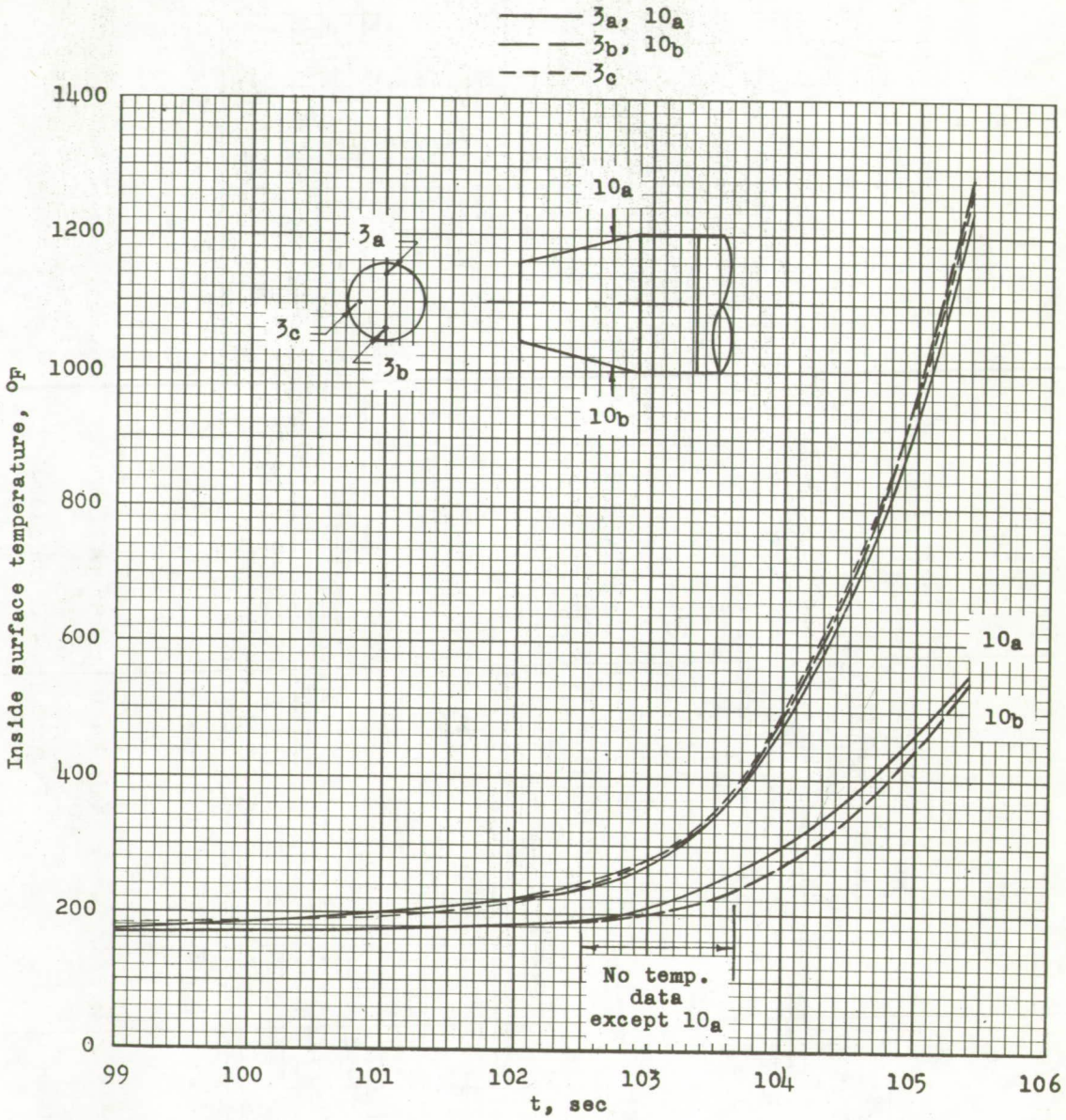


Figure 16.- Comparison of measured temperatures at symmetrical locations.

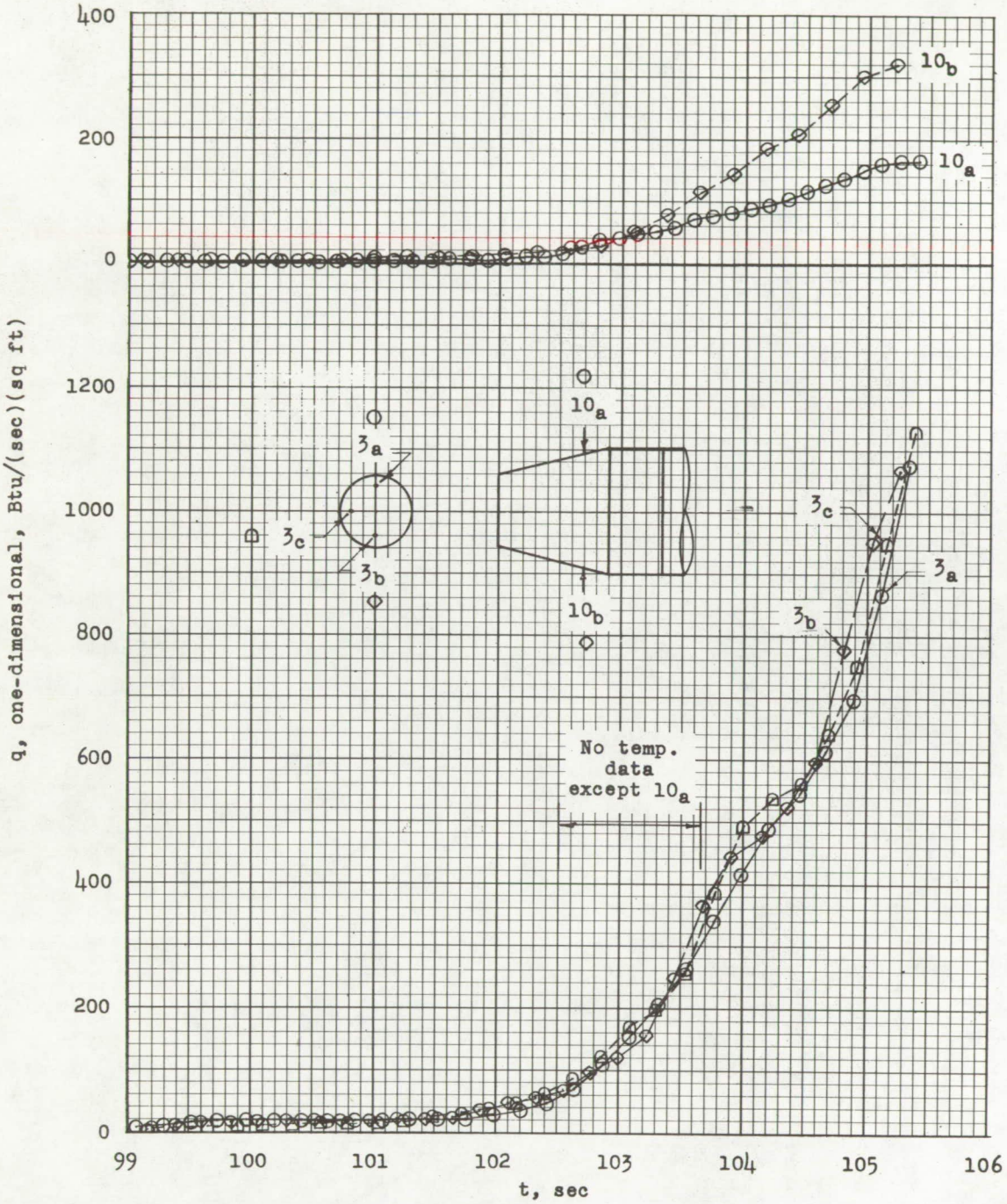


Figure 17.- Comparison of one-dimensional heating rates at symmetrical stations.